Nonlinear Susceptibilities of Donor–Acceptor Conjugated Systems: Coupled-Oscillator Representation

Guanhua Chen and Shaul Mukamel*

Contribution from the Center for Photoinduced Charge Transfer, Department of Chemistry, University of Rochester, Rochester, New York 14627

Received September 12, 1994[⊗]

Abstract: A coupled harmonic oscillator picture is developed for the nonlinear optical response of donor–acceptor substituted conjugated polyenes using the reduced single electron density matrix calculated within the time-dependent Hartree–Fock (TDHF) framework. The mechanism of the optical response is related to a few dominant oscillators which represent collective electron–hole excitations. The nature of these oscillators is analyzed. The optimization of the off-resonant nonlinear susceptibilities $\beta(0)$ and $\gamma(0)$ and the roles of Coulomb and exchange interactions are investigated.

I. Introduction

Conjugated polymers possess large nonlinear optical susceptibilities, and are good candidates for optical devices. Their nonlinear optical properties have therefore attracted considerable research activity.[1–9] In addition, being one-dimensional systems, electron correlations have strong effects on their optical properties.[10] This makes them ideal model systems for investigating strong electron–electron correlations.

Various computational techniques have been applied to the study of nonlinear optical properties of conjugated polymers. The finite-field approach is used to calculate the static polarizabilities.[1,11–14] It has been employed frequently for large molecules at the semiempirical and Hartree–Fock levels. The time-dependent Hartree–Fock (TDHF) method, formulated using either the wave function[15–17] or the one-particle density matrix[6,7] in the presence of an external field, may be used to calculate the static as well as the dynamic polarizabilities. The sum-over-states (SOS) procedure has been widely used as well, in particular for identifying the excited states which dominate the resonant response.[2,4,5,18] Electron correlation effects may be incorporated into the states by configuration interaction (CI). However, this requires extensive computer effort even for relatively small systems, because wave functions of all excited states in the frequency range of interest need to be calculated. To avoid this difficulty, the independent electron approximation [employing the Hückel or the Su–Schrieffer–Heeger (SSH) model] is frequently used.[19–22] Single excitation configuration interaction (SCI), known in nuclear physics as the Tamm–Dancoff approximation (TDA), may be employed to calculate the excited states. It neglects correlations in the ground state and assumes that the stationary Hartree–Fock ground state $|\Psi_{HF}\rangle$ is a good approximation for the real ground state. It proceeds to calculate the excited states by exciting one electron out of the occupied orbitals, and the excited state is represented by a linear combination of the single electron excitations: $a_p^+ a_h|\Psi_{HF}\rangle$, where a_p^+ and a_h are the creation and annihilation operators for unoccupied and occupied molecular orbitals. $a_p^+ a_h$ is denoted as the *particle–hole* (*ph*) transition. Techniques that incorporate ground state as well as excited state correlations include the doubly excited CI (DCI), the singly and doubly excited CI (SDCI), the independent electron pair approximation (IEPA), and the coupled-cluster approximation (CCA).[15,23]

An alternative approach is to treat electrons as harmonically bound particles. This Drude oscillator model has been long used to calculate linear spectra.[24,25] To describe optical nonlinearities, Bloembergen suggested to add a cubic anharmonic

[⊗] Abstract published in *Advance ACS Abstracts*, April 15, 1995.

(1) André, J. M.; Delhalle, J.; Brédas, J. L. *Quantum Chemistry Aided Design of Organic Polymers. An Introduction to the Quantum Chemistry of Polymers and its Applications*; World Scientific: Singapore, 1991.
(2) Chemla, D. S.; Zyss, J. *Nonlinear Optical Properties of Organic Molecules and Crystals*; Academic: New York, 1987.
(3) Samuel, I. D. W.; Ledoux, I.; Dhenaut, C.; Zyss, J.; Fox, H. H.; Schrock, R. R.; Silbey, R. J. *Science* **1994**, *265*, 1070.
(4) (a) Garito, A.; Shi, R. F.; Wu, M. *Phys. Today* **1994**, May, 51. (b) Rodenberger, D. C.; Heflin, J. R.; Garito, A. F. *Nature* **1992**, *359*, 309.
(5) (a) Etemad, S.; Soos, Z. G. In *Spectroscopy of Advanced Materials*; Clark, R. J. H., Hester, R. E., Eds.; Wiley: New York, 1991; p 87. (b) Soos, Z. G.; Ramesesha, S.; Galvao, D. S.; Etemad, S. *Phys. Rev. B* **1993**, *47*, 1742.
(6) Takahashi, A.; Mukamel, S. *J. Chem. Phys.* **1994**, *100*, 2366.
(7) (a) Mukamel, S.; Takahashi, A.; Wang, H. X.; Chen, G. *Science* **1994**, *266*, 251. (b) Chen, G.; Takahashi, A.; Mukamel, S. *Proc. SPIE* **1994**, *2143*, 142.
(8) (a) Marder, S. R.; Perry, J. W.; Bourhill, G.; Gorman, C. B.; Tiemann, B. G.; Mansour, K. *Science* **1993**, *261*, 186. (b) Marder, S. R.; Gorman, C. B.; Mayers, F.; Perry, J. W.; Bourhill, G.; Brédas, J. L.; Pierce, B. M. *Science* **1994**, *265*, 632.
(9) Risser, S. M.; Beratan, D. N.; Marder, S. R. *J. Am. Chem. Soc.* **1993**, *115*, 7719.
(10) Ohmine, I.; Karplus, M.; Schulten, K. *J. Chem. Phys.* **1978**, *68*, 2298.
(11) Kurtz, H. A.; Stewart, J. J. P.; Dieter, K. M. *J. Comput. Chem.* **1990**, *11*, 82.
(12) Sim, F.; Chin, S.; Dupuis, M.; Rice, J. *J. Phys. Chem.* **1993**, *97*, 1158.
(13) Karna, P. S.; Laskowski, Z.; Talapatra, G. B.; Prasad, P. N. *J. Phys. Chem.* **1991**, *95*, 6508.
(14) Cohen, H. D.; Roothaan, C. C. J. *J. Chem. Phys.* **1965**, *43*, S34.
(15) Sekino, H.; Bartlett, R. J. *J. Chem. Phys.* **1986**, *85*, 976.
(16) (a) Karna, S. P.; Dupuis, M. *J. Comput. Chem.* **1991**, *12*, 487. (b) Karna, S. P.; *et al. Phys Rev. A* **1992**, *45*, 2763.
(17) Langhoff, P. W.; Epstein, S. T.; Karplus, M. *Rev. Mod. Phys.* **1972**, *44*, 602.
(18) Orr, B. J.; Ward, J. F. *Mol. Phys.* **1971**, *20*, 513.
(19) Agrawal, G. P.; Cojan, C.; Flyzanis, C. *Phys. Rev. B* **1978**, *16*, 776.
(20) Wu, W. K. *Phys. Rev. Lett.* **1988**, *61*, 1119.
(21) Yu, J.; *et al. Phys. Rev. B* **1989**, *39*, 12814.
(22) Sun, X.; Nasu, K.; Wu, C. *Q. Appl. Phys. B* **1992**, *54*, 170.
(23) Szabo, A.; Ostlund, N. A. *Modern Quantum Chemistry*; McGraw-Hill: New York, 1989.
(24) (a) Lorentz, H. A. *The Theory of Electrons*; Dover: New York, 1952. (b) Rosenfeld, L. *Theory of Electrons*; North-Holland: Amsterdam, 1951.
(25) (a) Kuhn, H.; Huber, W. *Helv. Chim. Acta* **1959**, *42*, 363. (b) Kuhn, H.; Kuhn, C. *Chem. Phys. Lett.* **1993**, *204*, 206.

0002-7863/95/1517-4945$09.00/0

term.[26] This was proposed as a qualitative back of envelope model. To accurately describe nonlinear optical processes in conjugated systems, a first principle computational procedure is required. The reduced single electron density matrix carries information on charge distributions and chemical bonding.[27-29] Its diagonal elements are the electron densities whereas the off-diagonal elements represent electron coherences or bonding. This is much simpler compared with the full electronic wave function. A coupled harmonic oscillator picture based on the TDHF approximation for the reduced single electron density matrix has been developed for conjugated polymers.[6,7,30,31] It starts from a microscopic Hamiltonian. Using the Heisenberg equation of motion for a reduced density matrix, it rigorously maps the nonlinear optical response to the dynamics of a set of anharmonic oscillators. It relates the optical properties directly to the motions of electron–hole pairs, and avoids calculating the many-body wave functions. Thus, the necessary computation effort is greatly reduced compared to other methods.[6] More importantly, this approach identifies the key sources of anharmonic couplings, provides a new perspective on the mechanism of nonlinear optical processes, and offers a novel unified physical picture of the optical response in terms of electronic normal modes. It has been applied to predict the saturation length of the third-order polarizability γ,[7,30] and to study nonlinear optical processes in both the frequency[6] and time domains.[31]

Conjugated polymers with donor and acceptor substitutions often show large first-order as well as second-order hyperpolarizabilities. Much experimental and theoretical effort has focused on increasing the off-resonant hyperpolarizabilities by carefully designed substitutions.[8,9,32-34] Marder and co-workers[8] have investigated the structure–property relations for several classes of donor–acceptor conjugated polymers, and proposed a correlation between polarizabilities and the bond length alternation (BLA), which provided some simple guidelines for the synthesis of materials with large off-resonant hyperpolarizabilities.

In this paper we apply the coupled harmonic oscillator picture to calculate the first- and second-order off-resonant hyperpolarizabilities $\beta(0)$ and $\gamma(0)$ of donor–acceptor conjugated polymers. We study how to maximize the magnitudes of $\beta(0)$ and $\gamma(0)$, and investigate the separate roles of Coulomb and exchange interactions in the nonlinear optical properties. In section II, we present the electronic harmonic oscillator (HO) (or electronic normal mode) representation, derive the equations of motion for the oscillators, and discuss their general properties. In section III, we calculate the ground state properties of conjugated polyenes with donor and acceptor substitutions. In section IV, we evaluate the off-resonant polarizabilities $\alpha(0)$, $\beta(0)$, and $\gamma(0)$ and investigate the roles of different anharmonic couplings. In section V, we analyze the characters of the relevant oscillators and connect them to the molecular orbital representation. The results are finally summarized in section VI.

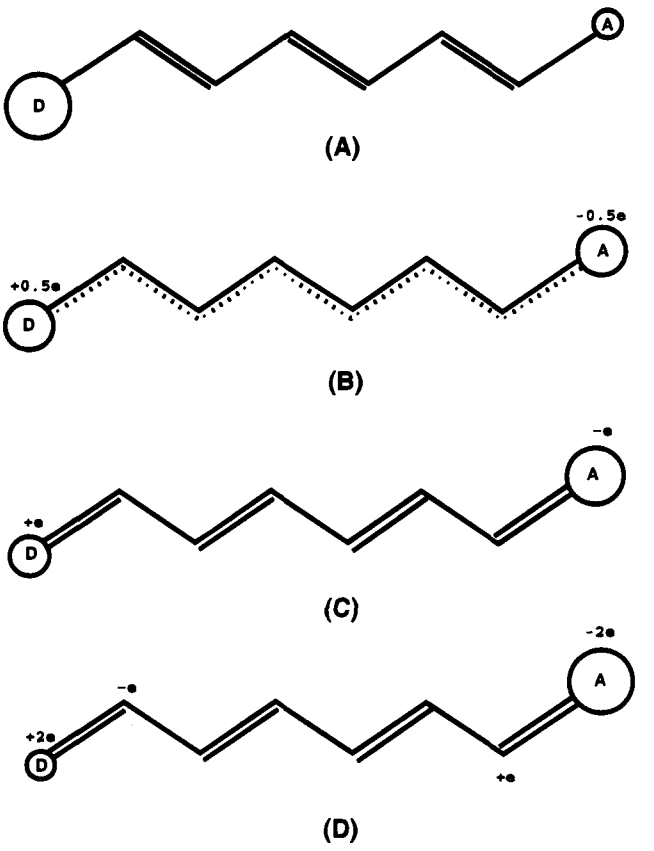

Figure 1. Possible electronic structures of the eight-site system: (A) neutral case without charge transfer; (B) half of an electron transferred; (C) one electron transferred; (D) two electrons transferred.

II. Electronic Harmonic Oscillator Representation

Our system is a conjugated polyene, substituted with a donor and an acceptor at each end (Figure 1). We model it as an N-electron N-site system consisting of a donor, an acceptor, and $N-2$ bridge sites. The donor and acceptor carry nuclear charges of $+2e$ and 0, respectively, whereas the charge on each bridge site is $+e$, where $-e$ is the charge of an electron. We adopt the Pariser–Parr–Pople (PPP) Hamiltonian for the system which is known to capture the essential electronic properties of the π electronic system[5-7,10,30,31,35]

$$H = H_{SSH} + H_C + H_{ext} \tag{1}$$

H_{SSH} is the Su–Schrieffer–Heeger (SSH) Hamiltonian, which consists of the Hückel Hamiltonian with electron–phonon coupling.

$$H_{SSH} = \sum_{n,m,\sigma} t_{mn}\hat{\varrho}^{\sigma}_{nm} + \sum_{n}(1/2)K(x_n - \bar{x})^2 \tag{2}$$

where $\hat{\varrho}^{\sigma}_{nm} = a^{+}_{m\sigma}a_{n\sigma}$. $a^{+}_{m\sigma}$ ($a_{n\sigma}$) is an electron creation (annihilation) operator with spin σ, t_{nn} is the energy at the nth site (including atomic orbital energy and the Coulomb integral between an electron and nuclei), t_{mn} ($m \neq n$) is the electron hopping matrix element between the nth and mth atoms, K is the σ-bond force constant, x_n is the nth bond length along the chain axis z, and $\bar{x}$ is the equilibrium bond length. Assuming

(26) Bloembergen, N. *Nonlinear Optics*; Benjamin: New York, 1965; pp 5–8.
(27) Davidson, E. R. *Reduced Density Matrices in Quantum Chemistry*; Academic Press: New York, 1976.
(28) McWeeny, R.; Sutcliffe, B. T. *Methods of Molecular Quantum Mechanics*; Academic Press: New York, 1976.
(29) Löwdin, P. O. *Phys. Rev.* **1955**, *97*, 1474.
(30) Mukamel, S.; Wang, H. X. *Phys. Rev. Lett.* **1992**, *69*, 65.
(31) (a) Hartmann, M.; Mukamel, S. *J. Chem. Phys.* **1993**, *99*, 1597. (b) Hartmann, M.; Chernyak, V.; Mukamel, S. *Phys. Rev. B*, in press.
(32) Kohler, B. E.; Spangler, C. W.; Westerfield, C. *J. Chem. Phys.* **1991**, *94*, 908.
(33) Blanchard-Desce, M.; Lehn, J.-M.; Barzoukas, M.; Ledoux, I.; Zyss, J. *Chem. Phys.* **1994**, *181*, 281.
(34) Lu, D.; Chen, G.; Perry, J. W.; Goddard, W. A., III. *J. Am. Chem. Soc.*, in press.
(35) Linderberg, J.; Ohrn, Y. *Propagators in Quantum Chemistry*; Academic Press: New York, 1973. Fukutome, H. *J. Mol. Struct.: THEOCHEM* **1989**, *188*, 337 and references therein.

that an electron can only hop between nearest neighbors, we have

$$t_{nm} = \begin{cases} \epsilon_n - \sum_{m'} v_{nm'} Z_{m'} & m = n \\ \bar{\beta} - \beta' \Delta z_n & m = n+1 \\ 0 & \text{otherwise} \end{cases}$$

Here ϵ_n is the atomic energy of the nth site, v_{nm} is a repulsion between the nth and mth sites, Z_m is the nuclear charge of the mth site (in units of e), $\bar{\beta}$ is the mean transfer integral, β' is the electron–phonon coupling constant, and Δz_n is the bond length deviation from its equilibrium value. We assume that $\epsilon_1 = \epsilon_D$, $\epsilon_N = \epsilon_A$, and all other atomic energies are zero, *i.e.*, $\epsilon_n = 0$ ($n = 2, ..., N-1$). v_{nm} is given by the Ohno formula

$$v_{nm} = \frac{U}{[1 + (r_{nm}/a_0)^2]^{1/2}} \tag{3}$$

where r_{nm} is the distance between nth and mth sites, a_0 is a characteristic length, and U is the on-site (Hubbard) repulsion

$$U = U_0/\epsilon \tag{4}$$

ϵ is the static dielectric constant representing the screening by σ electrons, and U_0 is the unscreened on-site repulsion.

The Coulomb interaction H_C is given by

$$H_C = \sum_n U \hat{\varrho}^{\uparrow}_{nn} \hat{\varrho}^{\downarrow}_{nn} + (1/2) \sum_{n,m,\sigma,\sigma'}^{n \neq m} v_{nm} \hat{\varrho}^{\sigma}_{nn} \hat{\varrho}^{\sigma'}_{mm} + (1/2) \sum_{m \neq n} v_{nm} Z_n Z_m \tag{5}$$

The three terms in H_C represent the on-site Coulomb interaction for electrons, the off-site Coulomb interaction, and the Coulomb repulsion among nuclei, respectively. The parameters are given in ref 6; $a_0 = 1.2935$ Å, $U_0 = 11.13$ eV, $\bar{\beta} = -2.4$ eV, $\beta' = -3.5$ eV Å^{-1}, $K = 30$ eV·Å^{-2}, $\bar{x} = 1.41$ Å, and $\epsilon = 1.5$. These were adjusted to reproduce the experimental optical transition energy (2.0 eV) for polyacetylene.[6] We expect the donor–acceptor substitution to affect primarily the π electrons and not the σ electrons. Consequently, we held ϵ fixed in the following calculations. An improved parameterization which can, *e.g.*, take into account the spatial dependence of ϵ can be made using effective Hamiltonian techniques.[1,36] This goes beyond the scope of the present calculations.

H_{ext} represents the interaction between the π electrons and an external electric field $\mathcal{E}(t)$, polarized along the chain z axis. Within the dipole approximation we have

$$H_{ext} = -\mathcal{E}(t)\hat{\mathcal{P}} \tag{6}$$

where $\hat{\mathcal{P}}$ is the polarization operator

$$\hat{\mathcal{P}} = -e \sum_{n,\sigma} z(n) \hat{\varrho}^{\sigma}_{nn} \tag{7}$$

and $z(n)$ is the z coordinate of the nth atom.

The one-electron density matrix element $\varrho^{\sigma}_{nm}(t) \equiv \langle \hat{\varrho}^{\sigma}_{nm} \rangle$ (*i.e.*, the expectation value of $\hat{\varrho}^{\sigma}_{nn}$) obeys the exact Heisenberg equation of motion,

$$i\hbar \dot{\varrho}^{\sigma}_{nm}(t) = \sum_i [t_{ni}\varrho^{\sigma}_{im}(t) - t_{im}\varrho^{\sigma}_{ni}(t)] + U[\langle \hat{\varrho}^{-\sigma}_{nn} \hat{\varrho}^{\sigma}_{nm} \rangle - \langle \hat{\varrho}^{-\sigma}_{mm} \hat{\varrho}^{\sigma}_{nm} \rangle] + (1/2) \sum_{i,\sigma'}^{i \neq n} v_{ni} (\langle \hat{\varrho}^{\sigma'}_{ii} \hat{\varrho}^{\sigma}_{nm} \rangle + \langle \hat{\varrho}^{\sigma}_{nm} \hat{\varrho}^{\sigma'}_{ii} \rangle) - (1/2) \sum_{i,\sigma'}^{i \neq m} v_{mi} (\langle \hat{\varrho}^{\sigma'}_{ii} \hat{\varrho}^{\sigma}_{nm} \rangle + \langle \hat{\varrho}^{\sigma}_{nm} \hat{\varrho}^{\sigma'}_{ii} \rangle) + e[z(n) - z(m)] \mathcal{E}(t) \varrho^{\sigma}_{nm}(t) \tag{8}$$

Assuming that the wave function may be represented by a single Slater determinant at all times results in the Hartree–Fock factorization,[37]

$$\langle \hat{\varrho}^{\sigma}_{nm} \hat{\varrho}^{\sigma'}_{ij} \rangle = \varrho^{\sigma}_{nm}(t) \varrho^{\sigma'}_{ij}(t) - \delta_{\sigma,\sigma'} \varrho^{\sigma}_{im}(t) \varrho^{\sigma'}_{nj}(t) + \delta_{\sigma,\sigma'} \delta_{j,n} \varrho^{\sigma}_{im}(t) \tag{9}$$

Combining eqs 8 and 9 yields the following closed nonlinear self-consistent equation of motion for the one-electron density matrix $\boldsymbol{\varrho}^{\sigma}(t)$:

$$i\hbar \dot{\boldsymbol{\varrho}}^{\sigma}(t) = [\mathbf{h}^{\sigma}(t) + \bar{\mathbf{f}}(t), \boldsymbol{\varrho}^{\sigma}(t)] \tag{10}$$

where $\mathbf{h}^{\sigma}$ and $\bar{\mathbf{f}}$ are $N \times N$ matrices,

$$h^{\sigma}_{nm}(t) = t_{nm} + \delta_{n,m} \sum_{l,\sigma'} v_{nl} \varrho^{\sigma'}_{ll}(t) - v_{nm} \varrho^{\sigma}_{nm}(t) \tag{11}$$

and

$$\bar{f}_{nm}(t) = \delta_{n,m} ez(n)\, \mathcal{E}(t) \tag{12}$$

In the remainder of this paper, we shall consider only spin symmetric (singlet) excitations, and thus omit the spin index. We partition the density matrix into two components:

$$\boldsymbol{\varrho}(t) = \boldsymbol{\varrho}^{(0)} + \delta\boldsymbol{\varrho}(t) \tag{13}$$

where $\boldsymbol{\varrho}^{(0)}$ is the one-electron density matrix representing the Hartree–Fock ground state and $\delta\boldsymbol{\varrho}(t)$ is induced by the driving field. Similarly, the Fock operator $\mathbf{h}$ is decomposed in the form

$$\mathbf{h}(t) = \mathbf{h}^{(0)} + \delta\mathbf{h}(t) \tag{14}$$

where

$$h^{(0)}_{nm} = t_{nm} + 2\delta_{n,m} \sum_l v_{nl} \varrho^{(0)}_{ll} - v_{nm} \varrho^{(0)}_{nm}$$

$$\delta h_{nm}(t) = 2\delta_{n,m} \sum_l v_{nl} \delta\varrho_{ll}(t) - v_{nm} \delta\varrho_{nm}(t) \tag{15}$$

We next show that the equations of motion map the electronic system onto a collection of anharmonic oscillators. To that end, we follow ref 6 and adopt Liouville space notation.[38,39] We rewrite $\delta\boldsymbol{\varrho}$ as an N^2 vector instead of an $N \times N$ matrix, and thus introduce a new vector space, denoted Liouville space. In Liouville space, ordinary operators are viewed as M-dimensional vectors ($M = N^2$, N being the number of basis states). After

(36) Martin, C. H.; Freed, K. F. *J. Chem. Phys.* **1994**, *101*, 4011.

(37) Ring, P.; Schuck, P. *The Nuclear Many-Body Problem*; Springer: New York, 1980.

(38) (a) Fano, U. *Rev. Mod. Phys.* **1957**, *29*, 74. (b) Zwanzig, R. *Lct. Theor. Phys.* **1961**, *3*, 106. (c) Zwanzig, R. *Physica* **1964**, *30*, 1109.

(39) Mukamel, S. *Principles of Nonlinear Optical Spectroscopy*; Oxford, New York, 1995.

some algebraic manipulation, eq 10 becomes

$$i\hbar\delta\dot{\boldsymbol{\varrho}} - \mathscr{L}\delta\boldsymbol{\varrho} = [\bar{\mathbf{f}}, \boldsymbol{\varrho}^{(0)}] + [\bar{\mathbf{f}}, \delta\boldsymbol{\varrho}] + [\delta\mathbf{h}, \delta\boldsymbol{\varrho}] \quad (16)$$

$$\mathscr{L}_{ij,mn}(\omega) = \delta_{j,n}h^{(0)}_{im} - \delta_{i,m}h^{(0)}_{jn} + 2\delta_{m,n}(\nu_{in} - \nu_{jn})\varrho^{(0)}_{ij} - \delta_{i,m}\nu_{in}\varrho^{(0)}_{jn} + \delta_{j,n}\nu_{jm}\varrho^{(0)}_{im} \quad (17)$$

where $\mathscr{L}$ is an $M \times M$ matrix which is an operator in Liouville space (also denoted superoperator or tetradic operator), $\delta\boldsymbol{\varrho}$ on the left side is an M-dimensional vector, and all terms on the right side are regarded as M-dimensional vectors. Formal manipulations in Liouville space become more transparent by introducing the following notation. An ordinary operator $\mathbf{A}$ (which is a vector in Liouville space) is represented by a double bracket ket $|\mathbf{A}\rangle\rangle$,[39] a scalar product of two vectors is defined as $\langle\langle\mathbf{B}|\mathbf{A}\rangle\rangle \equiv \mathrm{Tr}(\mathbf{B}^{+}\mathbf{A})$, and a matrix element of a superoperator $\mathscr{L}$ is $\langle\langle\mathbf{B}|\mathscr{L}|\mathbf{A}\rangle\rangle \equiv \mathrm{Tr}(\mathbf{B}^{+}\mathscr{L}\mathbf{A})$.

We next introduce a harmonic oscillator (HO) representation[6,30] by using the Liouville space eigenvectors $|\psi_\nu\rangle\rangle$ of the homogeneous equation

$$\mathscr{L}|\psi_\nu\rangle\rangle = \hbar\Omega_\nu|\psi_\nu\rangle\rangle \quad (18)$$

as a basis set, where Ω_ν are the corresponding eigenvalues. The eigenvectors $|\psi_\nu\rangle\rangle$ are defined by an $M \times M$ transformation matrix $\mathscr{U}^{-1}$ from the real space site (SITE) representation, *i.e.*,

$$|\psi_\nu\rangle\rangle = \sum_{m,n}\mathscr{U}^{-1}_{mn,\nu}|\hat{e}_{nm}\rangle\rangle \quad (19)$$

where $|\hat{e}_{nm}\rangle\rangle = a^{+}_m a_n$ is a basis vector in the SITE representation of Liouville space. Both $|\hat{e}_{nm}\rangle\rangle$ and $|\psi_\nu\rangle$ form a complete basis set in Liouville space, and we have

$$\sum_{nm}|\hat{e}_{nm}\rangle\rangle\langle\langle\hat{e}_{nm}| = \sum_{\nu}|\psi_\nu\rangle\rangle\langle\langle\psi_\nu| = 1 \quad (20)$$

We denote the component of $|\delta\boldsymbol{\varrho}\rangle\rangle$ along $|\psi_\nu\rangle\rangle$ by $\delta\varrho_\nu$, *i.e.*

$$|\delta\boldsymbol{\varrho}\rangle\rangle \equiv \sum_{\nu}\delta\varrho_\nu|\psi_\nu\rangle\rangle \quad (21)$$

with $\delta\varrho_\nu \equiv \langle\langle\psi_\nu|\delta\boldsymbol{\varrho}\rangle\rangle \equiv \mathrm{Tr}[\psi^{+}_\nu\delta\boldsymbol{\varrho}]$. Thus, the transformation between the SITE and HO representations is

$$\delta\varrho_\nu = \sum_{mn}\mathscr{U}_{\nu,mn}\delta\varrho_{mn} \quad (22)$$

with $\mathscr{U}^{-1}\mathscr{U} = 1$. In Appendix A, we transform the equation of motion (EOM) (eq 17) to the HO representation, and obtain

$$i\hbar\delta\dot{\varrho}_\nu - \hbar\Omega_\nu\delta\varrho_\nu - \mathscr{E}E_\nu = \mathscr{E}\sum_{\nu'}F_{\nu,\nu'}\,\delta\varrho_{\nu'} + \sum_{\nu',\nu''}(J_{\nu,\nu'\nu''} + K_{\nu,\nu'\nu''})\,\delta\varrho_{\nu'}\,\delta\varrho_{\nu''} \quad (23)$$

E_ν denotes the driving force induced by the external field, $F_{\nu,\nu'}$ represents a nonlinear coupling with the external field, $J_{\nu,\nu'\nu''}$ is related to direct Coulomb interaction, and $K_{\nu,\nu'\nu''}$ represents exchange Coulomb interaction. These coefficients are defined in Appendix A. If we neglect all terms on the right hand side, these equations become linear, $\delta\varrho_\nu$ will be proportional to $\mathscr{E}$, and all nonlinear polarizabilities β, γ, *etc.* vanish. The nonlinear response is thus induced by the field (F), the Coulomb (J) and exchange (K) anharmonic couplings. An important feature of the present formulation is that it makes it possible to investigate separately the contributions of various sources of nonlinearity.

It is further shown in Appendix A that for every eigenvector $|\psi_\nu\rangle\rangle$ with nonzero eigenvalue Ω_ν ($\neq 0$), there exists a conjugate eigenvector $|\psi_{\bar{\nu}}\rangle\rangle$ with eigenvalue $\Omega_{\bar{\nu}} = -\Omega_\nu$. Using the freedom we have in the choice of the relative phase of $|\psi_\nu\rangle\rangle$ and $|\psi_{\bar{\nu}}\rangle\rangle$, we take

$$\psi_{\bar{\nu}} = \psi^{\dagger}_\nu \quad (24)$$

i.e., $(\psi_{\bar{\nu}})_{nm} = (\psi_\nu)^{*}_{mn}$ and $\Omega_\nu = -\mu_{\bar{\nu}} \geq 0$. Making use of this symmetry, we introduce a new pair of operators

$$|\hat{Q}_\nu\rangle\rangle = \frac{|\psi_\nu\rangle\rangle + |\psi_{\bar{\nu}}\rangle\rangle}{\sqrt{2}} \quad (25)$$

$$|\hat{P}_\nu\rangle\rangle = -i\frac{|\psi_\nu\rangle\rangle - |\psi_{\bar{\nu}}\rangle\rangle}{\sqrt{2}} \quad (26)$$

whose expectation values are

$$Q_\nu \equiv \frac{\delta\varrho_\nu + \delta\varrho_{\bar{\nu}}}{\sqrt{2}} \quad (27)$$

$$P_\nu \equiv -i\frac{\delta\varrho_\nu - \delta\varrho_{\bar{\nu}}}{\sqrt{2}} \quad (28)$$

For zero frequency modes, $\Omega_\mu = 0$, the corresponding coordinates are

$$Q_\nu \equiv \delta\varrho_\nu/\sqrt{2}$$

$$P_\nu \equiv 0$$

As shown in Appendix A, eq 23 then transforms to the following form:

$$\dot{Q}_\nu - \Omega_\nu P_\nu = \sum_{\nu'}D^{\mathrm{b}}_{\nu,\nu'}P_{\nu'}\mathscr{E} + \sum_{\nu'\nu''}(C^{\mathrm{b}}_{\nu,\nu'\nu''} + X^{\mathrm{b}}_{\nu,\nu'\nu''})Q_{\nu'}P_{\nu''} \quad (29)$$

$$\dot{P}_\nu + \Omega_\nu Q_\nu - \bar{E}_\nu\mathscr{E} = -\sum_{\nu'}D^{\mathrm{a}}_{\nu,\nu'}Q_{\nu'}\mathscr{E} - \sum_{\nu'\nu''}(C^{\mathrm{a}}_{\nu,\nu'\nu''} + X^{\mathrm{a}}_{\nu,\nu'\nu''})Q_{\nu'}Q_{\nu''} + \sum_{\nu'\nu''}X^{\mathrm{c}}_{\nu,\nu'\nu''}P_{\nu'}P_{\nu''} \quad (30)$$

Q_ν and P_ν represent the coordinate and the momentum, respectively, of a harmonic oscillator with frequency Ω_ν. $\bar{E}_\nu$ represents linear coupling to the driving field. The terms on the right hand side of eqs 29 and 30 control the nonlinear dynamics of the system. Neglecting these nonlinear terms, eqs 29 and 30 can be combined to yield the equation of motion of a linearly driven harmonic oscillator[24]

$$\ddot{Q}_\nu + \Omega_\nu{}^2Q_\nu = \Omega_\nu\bar{E}_\nu\mathscr{E} \quad (31)$$

As in eq 23 we can classify the nonlinearities into three groups: $D^{\mathrm{s}}_{\nu,\nu'}$ (s = a, b), representing the nonlinear coupling between the external field and the oscillators, $C^{\mathrm{q}}_{\nu,\mathrm{nu}'\nu''}$ (q = a, b), are anharmonic couplings among oscillators due to direct Coulomb interaction, and $X^{\mathrm{r}}_{\nu,\nu'\nu''}$ (r = a, b, c, d), denoting anharmonic couplings due to exchange interaction. All of these coefficients are defined in Appendix A.

The oscillator picture can also be formulated in real space. To that end, we introduce the following pairs of operators:

$$|\hat{Q}_{ij}\rangle\rangle = \frac{|\hat{e}_{ij}\rangle\rangle + |\hat{e}_{ji}\rangle\rangle}{\sqrt{2}}$$

$$|\hat{P}_{ij}\rangle\rangle = -i\frac{|\hat{e}_{ij}\rangle\rangle - |\hat{e}_{ji}\rangle\rangle}{\sqrt{2}} \tag{32}$$

The corresponding expectation values are

$$Q_{ij} = \frac{\delta\varrho_{ij} + \delta\varrho_{ji}}{\sqrt{2}}$$

$$P_{ij} = -i\frac{\delta\varrho_{ij} - \delta\varrho_{ji}}{\sqrt{2}} \tag{33}$$

The EOM (eq 17) then becomes

$$\hbar\dot{Q}_{ij} - \sum_{m<n}(\mathscr{L}_{ij,mn} - \mathscr{L}_{ij,nm})P_{mn} = (\bar{f}_{ii} - \bar{f}_{jj})P_{ij} + \sum_k (v_{ik} - v_{jk})(2Q_{kk}P_{ij} - Q_{ik}P_{kj} - P_{ik}Q_{kj}) \tag{34}$$

$$\hbar\dot{P}_{ij} + \sum_{m<n}(\mathscr{L}_{ij,mn} + \mathscr{L}_{ij,nm})Q_{mn} + \sum_m \mathscr{L}_{ij,mm}Q_{mm} + 2(\bar{f}_{ii} - \bar{f}_{jj})\varrho^{(0)}_{ij} = -(\bar{f}_{ii} - \bar{f}_{jj})Q_{ij} - \sum_k (v_{ik} - v_{jk})(2Q_{kk}Q_{ij} - Q_{ik}Q_{kj} + P_{ik}P_{kj}) \tag{35}$$

Equations 34 and 35 are identical to eqs 29 and 30, but written in a different representation.

Equations 29 and 30 have several interesting features: (1) The system is mapped onto a collection of $N(N+1)/2$ coupled oscillators representing electronic normal modes. (2) Examination of $C^{q}_{\nu,n u'\nu''}$, $X^{r}_{\nu,\nu'\nu''}$, and $D^{s}_{\nu,\nu'}$ should reveal how various oscillators couple and contribute to the total polarization. This should also clarify how the three types of nonlinearities contribute to the hyperpolarizabilities and allow us to analyze their effects separately. In contrast, in the sum over states formulation, the analysis is made in terms of the molecular eigenvalues and their dipole matrix elements. (3) The dipole moment d_ν associated with the $|\hat{Q}_\nu\rangle\rangle$ oscillator is given by

$$d_\nu \equiv \langle\langle\hat{\mathscr{P}}|\hat{Q}_\nu\rangle\rangle = -2\sqrt{2}e\sum_m z(m)\mathscr{U}^{-1}_{mm,\nu} \tag{36}$$

where $\hat{\mathscr{P}}$ is the polarization operator given in eq 7. We choose the overall phase of $|\hat{Q}_\nu\rangle\rangle$ such that the dipole moment d_ν is non-negative. It follows from eq 24 that the momentum $|\hat{P}_\nu\rangle\rangle$ has a vanishing dipole moment. Thus, the polarization operator defined in eq 7 depends only on the coordinates $\hat{Q}_\nu$ but not on the momenta $\hat{P}_\nu$ and is given by

$$\hat{\mathscr{P}} = \sum_\nu d_\nu\hat{Q}_\nu \tag{37}$$

The nth order polarizability χ_n is given by

$$\chi_n = \sum_\nu d_\nu Q^{(n)}_\nu/\mathscr{E}^n \tag{38}$$

where $\chi_1 = \alpha$, $\chi_2 = \beta$, $\chi_3 = \gamma$, and $Q^{(n)}_\nu$ is the nth order of Q_ν in the external field $\mathscr{E}$. (4) The system has N zero frequency ($\Omega_\mu = 0$) modes (ZFM) (see Appendix B). For these modes, $\Omega_\mu = 0$, $P_\mu = 0$, and

$$\dot{Q}_\mu(t) = \sum_{\nu'} D^{b}_{\mu,\nu'}P_{\nu'}\mathscr{E} + \sum_{\nu'\nu''}(C^{b}_{\mu,\nu'\nu''} + X^{b}_{\mu,\nu'\nu''})Q_{\nu'}P_{\nu''} \tag{39}$$

It follows from this equation that these modes do not contribute to the linear polarizability since the terms on the right hand side are all nonlinear. Thus, $Q^{(1)}_\mu = 0$. When eq 39 is transformed to the frequency domain, both the left hand side and right hand side are proportional to ω as $\omega \to 0$ (see eq A16). Therefore, $Q^{(2)}_\mu$ and $Q^{(3)}_\mu$ are finite as $\omega \to 0$, and these modes contribute to $\beta(0)$ and $\gamma(0)$.

Following ref 31, we can define the oscillator strength f_ν of the νth harmonic oscillator, which is a measure of its contribution to the linear polarizability α. Starting with the linearized EOM (eq 31), and multiplying it by the dipole moment d_ν of the $|\hat{Q}_\nu\rangle\rangle$, we obtain the equation of a driven oscillator for the polarization,[24] *i.e.*,

$$\ddot{\mathscr{P}}_\nu = -\Omega_\nu^2\mathscr{P}_\nu + f_\nu\frac{e^2}{m_0}\mathscr{E} \tag{40}$$

where $\mathscr{P}_\nu \equiv d_\nu Q_\nu$ and the oscillator strength f_ν is defined as

$$f_\nu \equiv \sum_{m,n} f_\nu(m,n)$$

$$f_\nu(m,n) \equiv 4(m_0/\hbar)\Omega_\nu\sum_l z(l)[z(m) - z(n)]\mathscr{U}^{-1}_{ll,\nu}\mathscr{U}_{\nu,mn}\varrho^{(0)}_{mn}$$

$$\equiv \sqrt{2}(m_0/\hbar)\Omega_\nu d_\nu\mathscr{U}_{\nu,mn}[z(n) - z(m)]\varrho^{(0)}_{mn} \tag{41}$$

$f_\nu(m,n)$ is the oscillator strength density,[31] and m_0 is an effective mass which can be determined by imposing the Thomas–Reiche–Kuhn sum rule,[40]

$$\sum_\nu f_\nu = N \tag{42}$$

Using eq 40, the linear polarizability $\alpha(\omega)$ assumes the Drude oscillator form

$$\alpha(\omega) = \sum_{m,n}\alpha_{mn}(\omega) = \frac{e^2}{m_0}\sum_\nu\frac{f_\nu}{\Omega_\nu^2 - \omega^2} \tag{43}$$

with

$$\alpha_{mn}(\omega) = \frac{e^2}{m_0}\sum_\nu\frac{f_\nu(m,n)}{\Omega_\nu^2 - \omega^2} \tag{44}$$

III. Electronic Properties of the Ground State

In this section we calculate some basic properties of the system including the charge distributions, the bond order,[41] the bond order alternation, and the lowest absorption peak frequency Ω_0. These are important for interpreting the optical properties of conjugated polymers. In the next section we calculate the off-resonant polarizabilities $\alpha(0)$, $\beta(0)$, and $\gamma(0)$, and investigate their correlation with the equilibrium properties of the molecule.

The ground state charge distribution is

$$d^{(0)}_n \equiv 1 - 2\varrho^{(0)}_{nn} \tag{45}$$

Here $\varrho^{(0)}$ is the density matrix for the Hartree–Fock ground state and n is the site index.

(40) Bethe, H. A.; Salpeter, E. E. *Quantum Mechanics of One- and Two-electron Atoms*; Plenum: New York, 1977.

(41) Coulson, C. A. *Proc. R. Soc. London* **1939**, *A169*, 413.

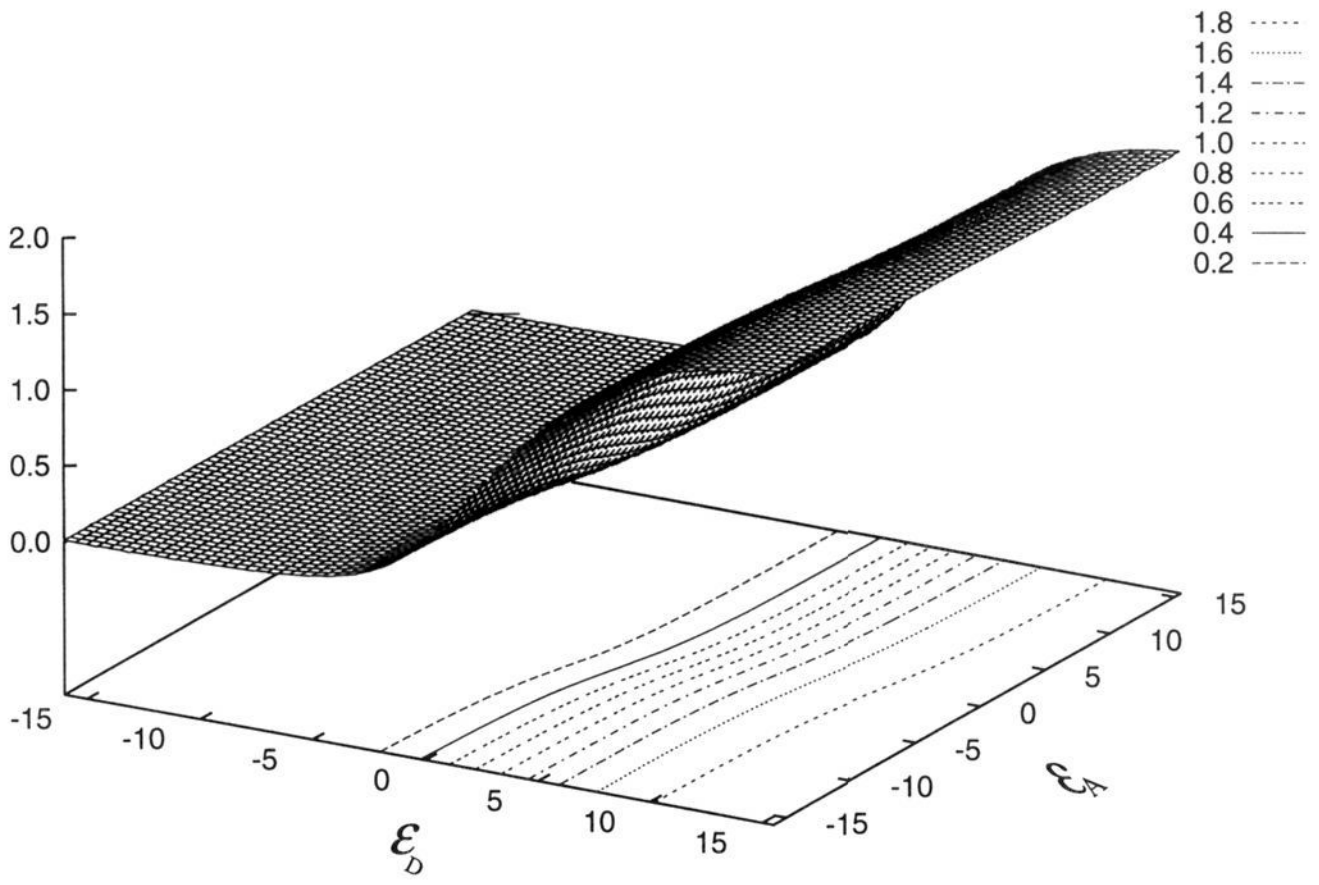

Figure 2. Donor ground state charge Q_D vs ϵ_D and ϵ_A. Q_D is primarily determined by ϵ_D and is insensitive to ϵ_A.

The bond order of the π bond between sites n and $n+1$ is related to the off-diagonal element of the ground state reduced density matrix,[41] and is defined as $(\varrho^{(0)}_{n,n+1} + \varrho^{(0)}_{n+1,n})/2$. The average bond order $\bar{p}^{(0)}$ is defined as

$$\bar{p}^{(0)} \equiv \frac{1}{2(N-1)}\sum_n (\varrho^{(0)}_{n,n+1} + \varrho^{(0)}_{n+1,n}) \tag{46}$$

The staggered bond order measures the alternating nature of chemical bonds in conjugated systems,

$$p^{(0)}_n \equiv (-1)^{n-1}(\varrho^{(0)}_{n,n+1} + \varrho^{(0)}_{n+1,n} - 2\bar{p}^{(0)}) \tag{47}$$

The $(-1)^{n-1}$ factor eliminates a change in sign on the right hand side due to alternation, and makes $p^{(0)}_n$ smooth. The average bond order alternation (BOA) is an important parameter in chemical bonding,

$$\begin{aligned}\mathrm{BOA} &\equiv \langle \varrho^{(0)}_{i,i+1} - \varrho^{(0)}_{i+1,i+2}\rangle \\ &= \frac{1}{N-4}\sum_{i=2,4,\ldots,N-4} (\varrho^{(0)}_{i,i+1} + \varrho^{(0)}_{i+2,i+3} - 2\varrho^{(0)}_{i+1,i+2})\end{aligned} \tag{48}$$

The superscript in all quantities represents the order with respect to the driving field, and zero order implies ground state properties. In the next section we consider quantities in kth order and analyze the optical response. The induced charge distribution to kth order in the field ($k = 1, 2, 3$), which is intimately related to the polarization, is

$$d^{(k)}_n \equiv -2\varrho^{(k)}_{nn} \tag{49}$$

We consider an eight-site ($N = 8$) substituted system made of a six carbon atom (hexatriene) bridge, a donor and an acceptor group at each end, and eight electrons. For comparison we also perform calculations for the unsubstituted isoelectronic octatetraene system.[42] By tuning ϵ_D and ϵ_A, we can change the geometry, bond order, and charge distribution of the system. We calculated the average bond order $\bar{p}^{(0)}$, staggered bond order $p^{(0)}_n$, BOA, charge distribution $d^{(0)}_n$, and optical frequency Ω_0. In all calculations, geometries are optimized within the Hartree–Fock approximation.[23]

Risser, Beratan, and Marder[9] employed a four-orbital Hückel model to describe a push–pull conjugated polymer (two bridge orbitals, one donor, and one acceptor). By exploring a wide range of parameters, they discussed the optimization of the magnitude of the off-resonant first hyperpolarizability $\beta(0)$. The following calculations differ from that study in the following respects. First, we include Coulomb interactions among electrons and nuclei as well as geometry optimization. Second, we also study the second hyperpolarizability γ. And third, we recast our results in terms of the electronic oscillator picture rather than the conventional eigenvalues and matrix elements of the dipole operator.

To illustrate the onset of charge transfer, we plot the charge at the donor site Q_D for different values of ϵ_D and ϵ_A in Figure 2. Q_D is primarily controlled by ϵ_D. This is because ϵ_D determines the energies of the donor electrons relative to the bridge. When ϵ_D is low, it is energetically favorable for electrons to remain at the donor site. As ϵ_D is increased, the donor electrons move to the bridge since this is energetically more favorable. When ϵ_D is negative and large, *i.e.*, the energy of the donor site is very low, $Q_D \approx 0$ and there is no electron transfer from the donor to the bridge or to the acceptor. At $\epsilon_D \approx 2$–4 eV, about one electron transfers from the donor to the bridge and acceptor. When the donor site energy is very high, both electrons transfer. For instance, at $\epsilon_D = 12$ eV, $Q_D \approx 1.9e$. In Figure 3, we show the charge at the acceptor site Q_A. It has characteristics similar to those of Q_D. It depends primarily on ϵ_A and shows only a weak dependence on ϵ_D, since ϵ_A controls the energies of electrons at the acceptor. At its large positive and negative values, Q_A is close to 0 and $-2e$, respectively. At $\epsilon_A = -6$ to -4 eV, $Q_A \approx 1e$. In Figure 4, we plot Ω_0 for different values of ϵ_D and ϵ_A. As charge transfer takes place, the electronic excitation energy is lowered, and the optical transition is red shifted. Around $(\epsilon_D,\epsilon_A) = (3.0,-2.0)$ eV, Ω_0 reaches its minimum value, ~2.6 eV. In this region $Q_D \approx 0.7e$ and $Q_A \approx 0.8e$; *i.e.*, less than one electron transfers from the donor to the acceptor.

In Figure 5, we display the BOA vs ϵ_D and ϵ_A. At low ϵ_D and high ϵ_A, the BOA ≈ 0.3 is large and positive. This implies bonding structure A in Figure 1. At high ϵ_D and low ϵ_A, BOA

(42) Buma, W. J.; Kohler, B. E.; Shaler, T. A. *J. Chem. Phys.* **1992**, *96*, 399.

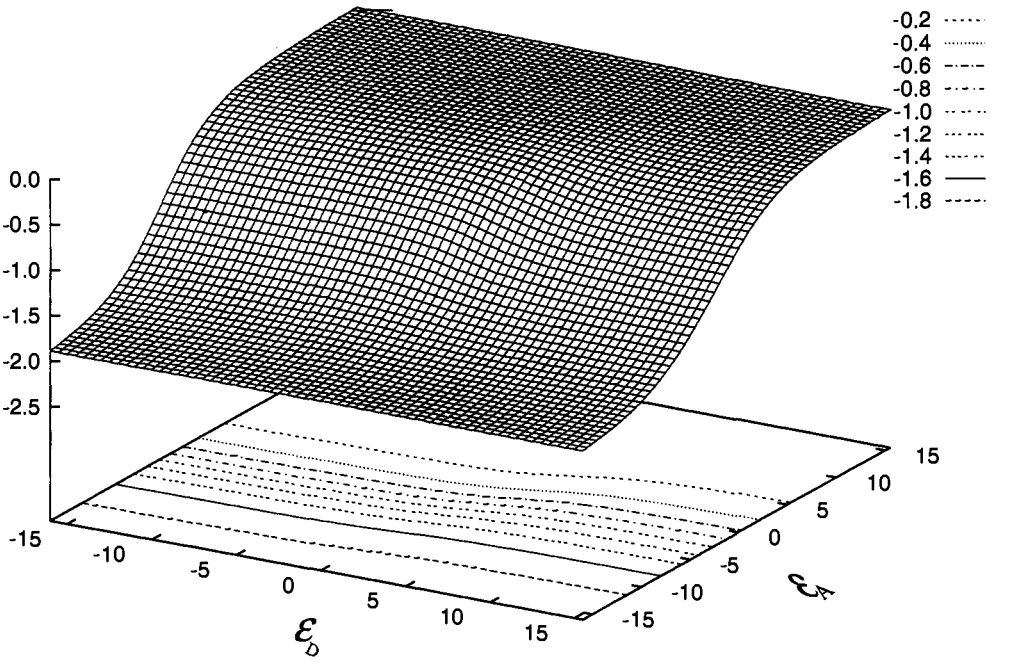

Fig. 3

Figure 3. Acceptor ground state charge Q_A vs ϵ_D and ϵ_A. Q_A is primarily determined by the value of ϵ_A and is insensitive to ϵ_D.

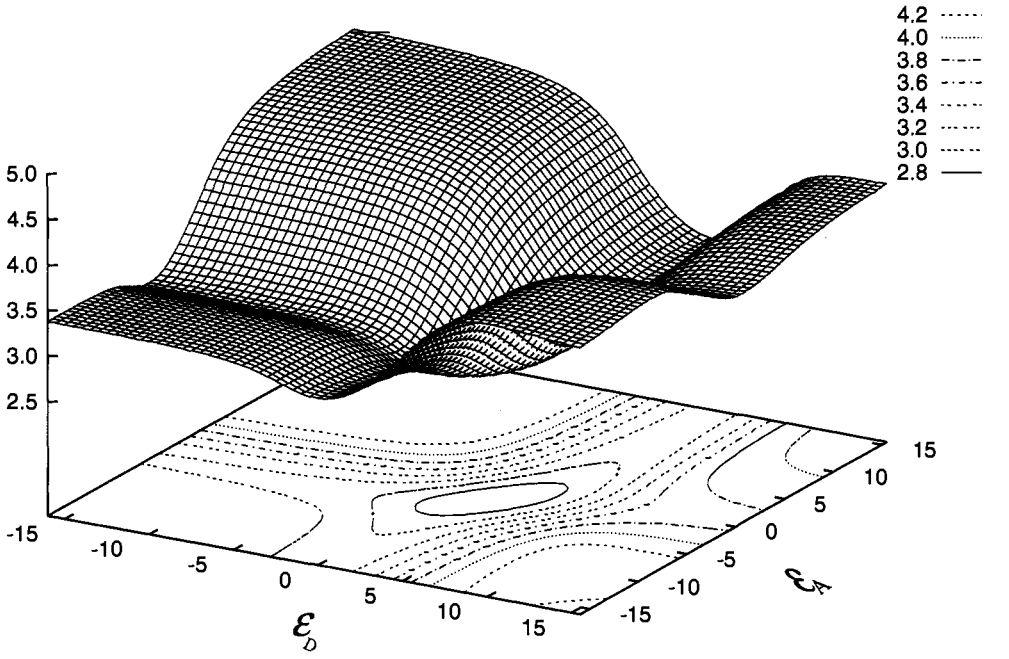

Figure 4. Frequency of the lowest absorption peak Ω_0 vs ϵ_D and ϵ_A. The minimum frequency is obtained for $(\epsilon_D, \epsilon_A) = (2, -2)$ eV.

≈ -0.3 is large and negative, which reflects the reverse bonding structure C or D (Figure 1). When BOA is close to zero, the structure is close to B, the cyanine limit. This classification has been suggested in ref 8.

In Figure 6 we display Q_D, Q_A, BOA, and Ω_0 for $\epsilon_D = -\epsilon_A$. The optical transition frequency Ω_0 attains its minimal value (maximum red shift) at $\epsilon_D = 2.625$ eV where $Q_D = 0.7e$ and $Q_A = -0.8e$. The BOA vanishes at a slightly different point ($\epsilon_D = 2$ eV). On the basis of an independent electron picture, we might expect Ω_0 to be minimal when the BOA vanishes. However, electron–electron correlations and geometry changes are responsible for the difference. We shall focus our subsequent analysis on the following points: $\epsilon_D = -\epsilon_A = -6.0$, 2.0, 2.25, 3.625, 4.375, and 10.0 eV. These will be denoted points E, F, G, H, I, and J, respectively. These points will be examined in the following figures and tables.

In Figure 7, we plot the average bond order $\bar{p}^{(0)}$ vs ϵ_D for $\epsilon_D = -\epsilon_A$. It peaks at point G, where BOA is approximately zero. In Figure 8, we plot the staggered bond order $p_n^{(0)}$ for points E, F, G, H, I, and J. At *E*, $p_n^{(0)} \approx -0.3$. This corresponds to structure A in Figure 1. At F and G, $p_n^{(0)}$ is close to zero which implies that electrons are delocalized along the chain [structure B]. At H, I, and J, p_n is positive, which means a bonding structure of forms C and D. In Figure 9, we plot the charge distribution $d_n^{(0)}$ for the same values of ϵ_D and ϵ_A used in Figure 8. The charge transferred from donor to acceptor increases with the D–A strength. At E, a very small charge is transferred, at H and I, approximately one electron is transferred, and at J, almost two electrons transfer. The bonding structure corresponding to points H and I is similar to C while the structure corresponding to point J is close to D.

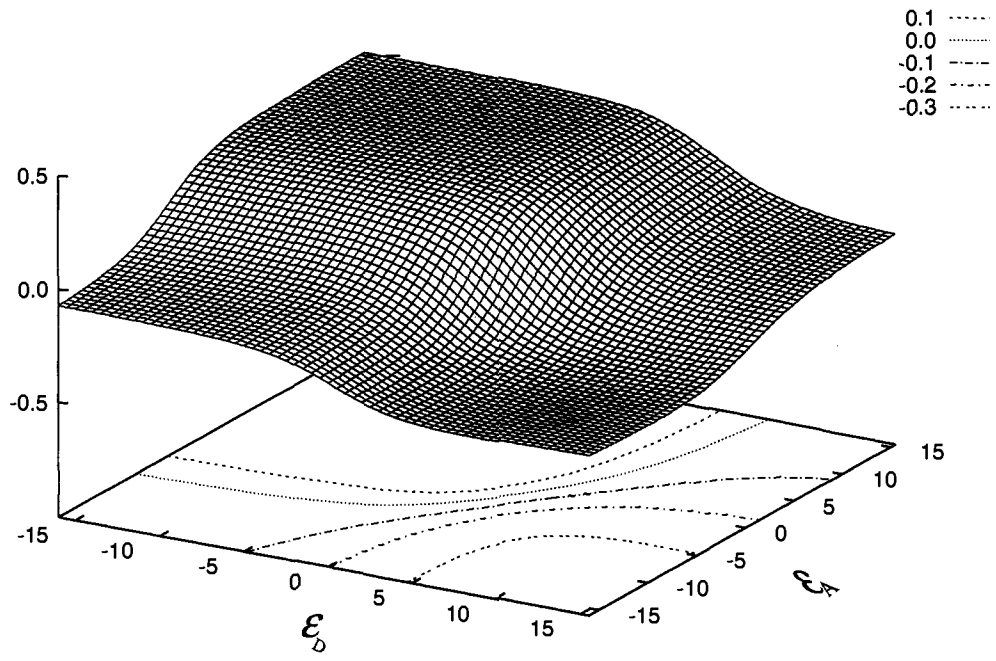

Fig. 5

Figure 5. Bond order alternation (BOA) vs ϵ_D and ϵ_A. Positive, zero, and negative BOAs correspond to structures A, B, and C or D of Figure 1, respectively.

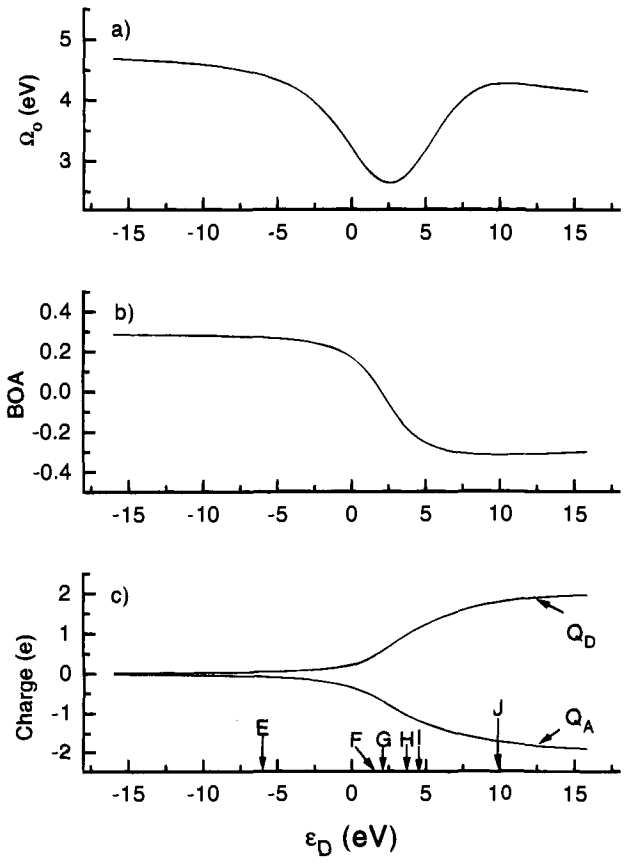

Figure 6. Ground state properties for $\epsilon_D = -\epsilon_A$: (a) frequency of the lowest absorption peak Ω_0; (b) bond order alternation (BOA) which vanishes at point F; (c) charges on the donor and acceptor Q_D and Q_A. Points E, F, G, H, I, and J stand for $\epsilon_D = -\epsilon_A = -6.0$, 2.0, 2.25, 3.625, 4.375, and 10.0 eV, respectively.

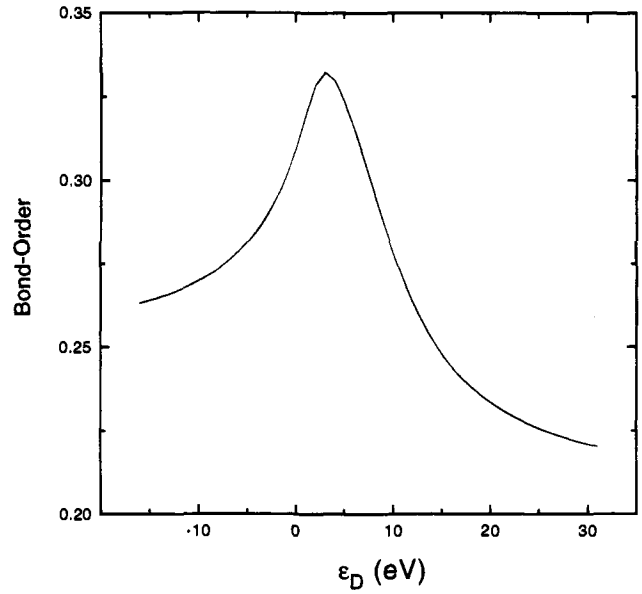

Figure 7. Average bond order $\bar{p}^{(0)}$ vs ϵ_D for $\epsilon_D = -\epsilon_A$. $\bar{p}^{(0)}$ peaks around point G.

IV. Off-Resonant Polarizabilities of Substituted Hexatriene

We now present the off-resonant polarizabilities $\alpha(0)$, $\beta(0)$, and $\gamma(0)$ at different values of ϵ_D and ϵ_A, correlate their magnitudes with the induced charge distributions at each order, and investigate their relationships with the ground state properties: Q_D, Q_A, BOA and Ω_0.

In Figure 10, we plot $\alpha(0)$ vs ϵ_D and ϵ_A. There is one peak at point G where the BOA is close to zero, the frequency Ω_0 is near its minimum, and about half an electron transfers from donor to acceptor. In Figure 11, we plot $\beta(0)$ vs ϵ_D and ϵ_A. It has one large positive peak around point H and one negative peak around $\epsilon_D = \epsilon_A = 0$. In Figure 12, we plot $\gamma(0)$ vs ϵ_D and ϵ_A. There are two positive peaks, a larger one at point I and a smaller one around (0, 0), and a negative peak around point F.

In Figure 13 we plot $\alpha(0)$, $\beta(0)$, and $\gamma(0)$ for $\epsilon_D = -\epsilon_A = -16$ to $+16$ eV. $\alpha(0)$ is maximized at G, and $\beta(0)$ reaches its maximum at H and minimum at 0.75 eV and vanishes around F. $\gamma(0)$ has a maximum at I and minimum at F, and is zero at 3.0 eV. For comparison, we calculated $\alpha(0)$, $\beta(0)$, and $\gamma(0)$

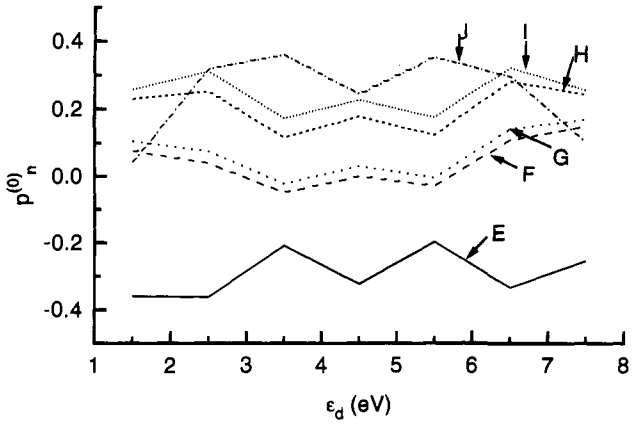

Figure 8. Staggered bond order $p_n^{(0)}$ for points E, G, H, I, and J. E corresponds to structure A in Figure 1, F and G correspond to B, and H, I, and J correspond to C or D.

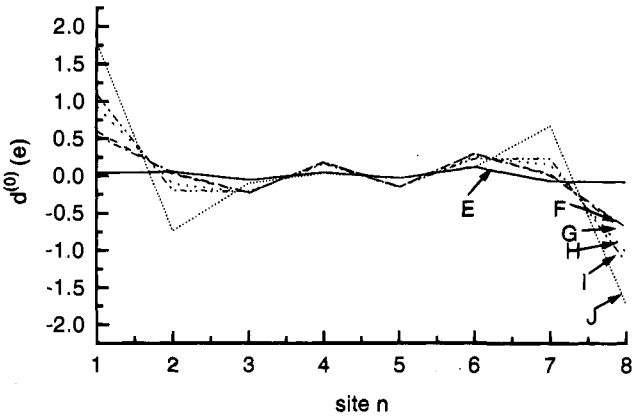

Figure 9. Charge distribution in the ground state $d_n^{(0)}$ for points E, F, G, H, I, and J. The charges at the donor and acceptor increase monotonically with increased donor–acceptor strength.

for octatetraene, and the results are given by the arrows in Figure 13. We found $\alpha(0) = 2.614 \times 10^{-22}$ esu which is less than half of the maximum $\alpha(0)$ value, $\beta(0) = 0$, and $\gamma(0) = 0.3312 \times 10^{-33}$ esu which is about one-fifth of the maximum value of $\gamma(0)$ for the substituted hexatriene. These illustrate how donor and acceptor substitutions can increase the hyperpolarizabilities.[9]

In Figure 14, we show various characteristics of points E, F, G, H, I, and J. To explain the variation of $\alpha(0)$, we plot the first-order induced charge distribution $d_n^{(1)}$ in the bottom panel. We find that at E and J the induced charges at the donor and acceptor are small while at F, G, H, and I these charges are large. At F and G, the induced charges on the bridge are small. At H and I, these charges are moderate, but the corresponding induced dipole moments cancel, and the net dipole moment is opposite that from the donor and acceptor. At E and J, the induced dipole moments on the bridge cancel when added, and this leads to a small first-order polarization. Combining the contributions to the polarization from the donor–acceptor system and the bridge, we can rationalize why $\alpha(0)$ peaks around F and G.

To analyze the behavior of $\beta(0)$, we plot the second-order induced charge distribution $d_n^{(2)}$ in the middle panel. At E and J, these charges are small at both the bridge and the donor–acceptor, and this leads to $\beta(0) \approx 0$. At F and G, the second-order induced charges are small at the donor and the acceptor but quite large at the bridge. However, the corresponding dipole moments at the bridge cancel when added, and this leads to a near zero $\beta(0)$. At H and I, the induced charges are large at both bridge and donor–acceptor, which leads to large values of $\beta(0)$.

We next turn to $\gamma(0)$, and consider the third-order induced charge distribution $d_n^{(3)}$ shown in the top panel. At E and J, the third-order induced charges at both the bridge and the donor–acceptor are small, leading to a small $\gamma(0)$. At F and G, the induced charge is large at the donor and acceptor but small at the bridge. At I, the induced charge is large at both the bridge and donor–acceptor, which leads to a maximum value of $\gamma(0)$.

In order to use these results for developing a structure–polarization relationship, let us consider the following argument: Consider a conjugated polyene subjected to an external electric field $\mathcal{E}_{ext}$ along the chain, and plot $\alpha(0)$, $\beta(0)$, and $\gamma(0)$ vs the field: it then follows directly from their definitions that these

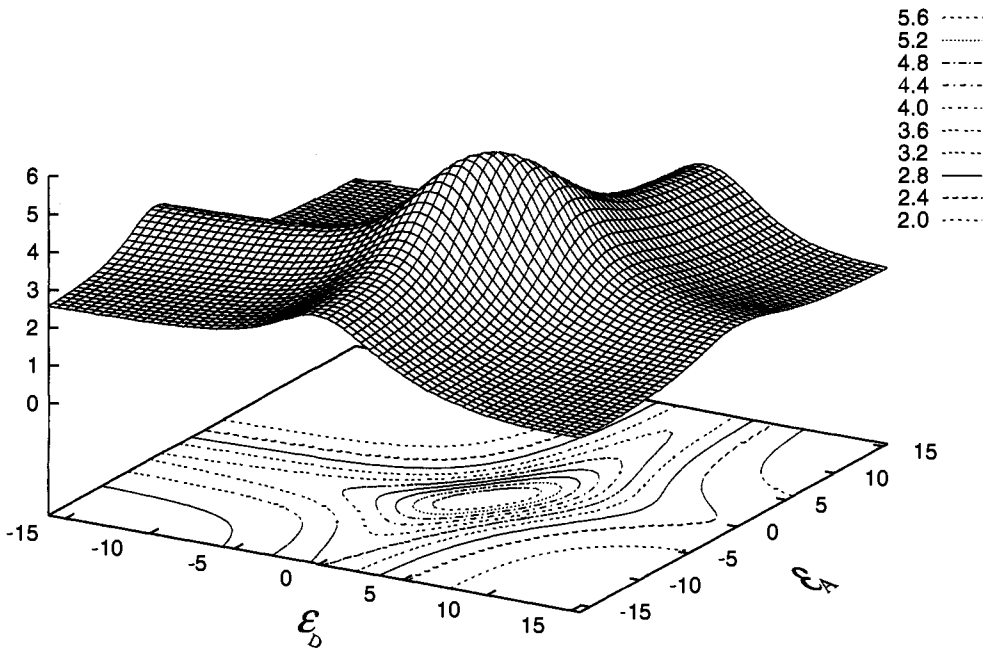

Fig. 10

Figure 10. $\alpha(0)$ (10^{-22} esu) vs ϵ_D and ϵ_A. $\epsilon_D = -16$ to $+16$ eV, and $\epsilon_A = -16$ to $+16$ eV. There is only one peak, around point G.

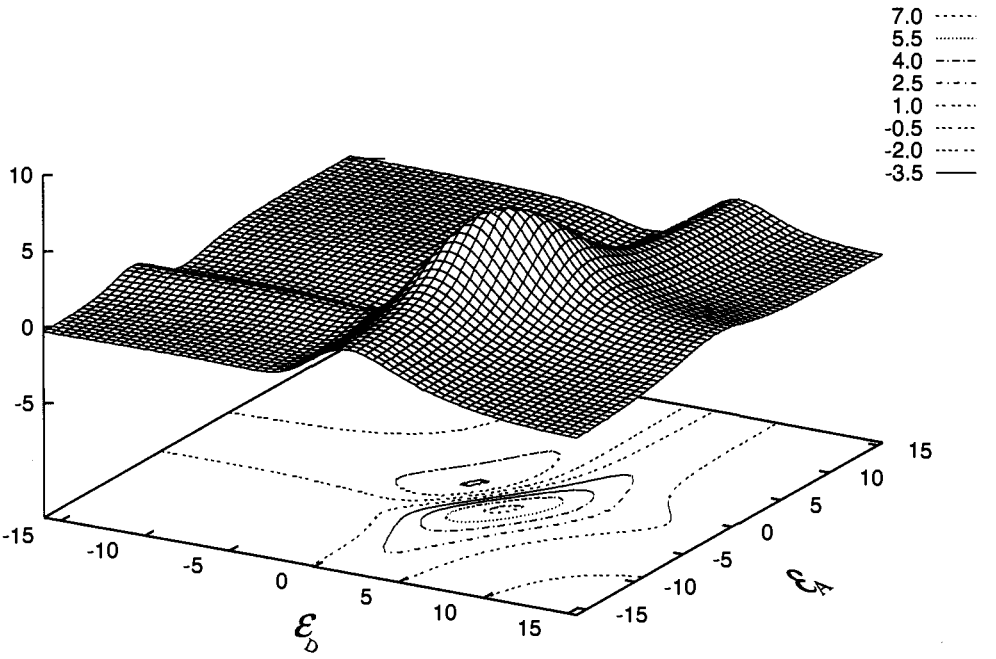

Figure 11. $\beta(0)$ (10^{-28} esu) vs ϵ_D and ϵ_A. There are one positive peak and one negative peak located at point H and (−0.5, 0.5). $\beta(0)$ vanishes around point F.

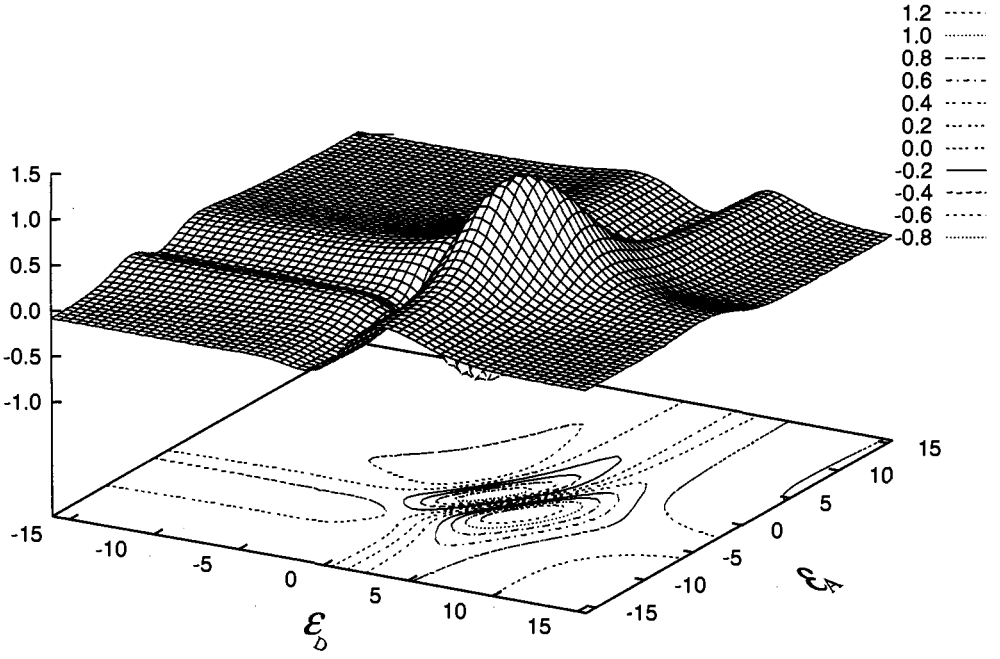

Figure 12. $\gamma(0)$ (10^{-33} esu) vs ϵ_D and ϵ_A. There are two positive peaks, located at point I (large peak) and around (0, 0). A negative peak is around point F.

quantities are related by simple derivatives,

$$\beta(0;\mathcal{E}_{ext}) = \frac{d\alpha(0;\mathcal{E}_{ext})}{d\mathcal{E}_{ext}}$$

$$\gamma(0;\mathcal{E}_{ext}) = \frac{d\beta(0;\mathcal{E}_{ext})}{d\mathcal{E}_{ext}} \qquad (50)$$

Assuming the effects of the donor and acceptor (or a solvent) can be approximated by an effective electric field along the chain, and that the BOA depends linearly on the field, we may expect a simple derivative relation among $\alpha(0)$, $\beta(0)$, and $\gamma(0)$ when plotted vs the BOA. To test this conjecture, we plot α-(0), $\beta(0)$, and $\gamma(0)$ vs BOA in Figure 15. Near zero BOA, α-(0) has a maximum, $\beta(0)$ is close to zero, and $\gamma(0)$ reaches its minimum. Thus, in the vicinity of zero BOA the derivative relationship holds approximately. However, this is not the case in general. For instance, $\beta(0)$ has a positive peak at BOA ≈ -0.2 and a negative peak at BOA ≈ 0.15, whereas the derivative of $\alpha(0)$ with respect to BOA does not show any peak at all. We thus conclude that the derivative relationship among $\alpha(0)$, $\beta(0)$, and $\gamma(0)$ holds only over a limited range of parameters. Marder and co-workers investigated a series of conjugated systems and used different polar solvents to modify their BOA.[8] They measured the off-resonant hyperpolarizabilities β and γ and found that with the change of BOA the values of $\beta(0)$ go through a positive peak, zero, and then a negative peak while $\gamma(0)$ goes from a positive peak to a negative peak and then to another positive peak. Our calculations are consistent with these observations.

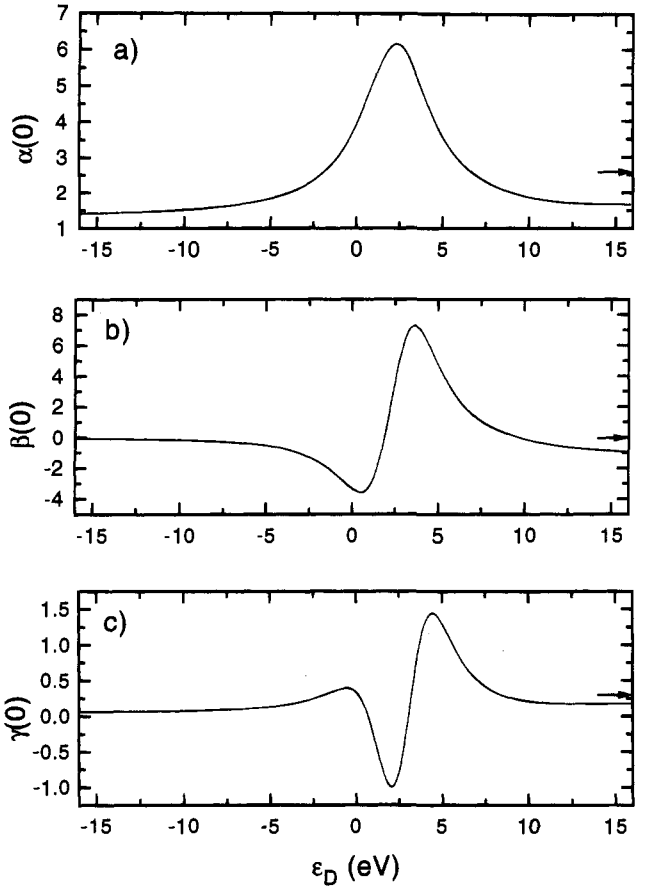

Figure 13. Off-resonant polarizabilities for $\epsilon_D = -\epsilon_A = -16.0$ to +16.0 eV: (a) $\alpha(0)$ has one peak; (b) $\beta(0)$ has a positive peak and a negative peak; (c) $\gamma(0)$ has two positive peaks and one negative one. Arrows represent the results of octatetraene.

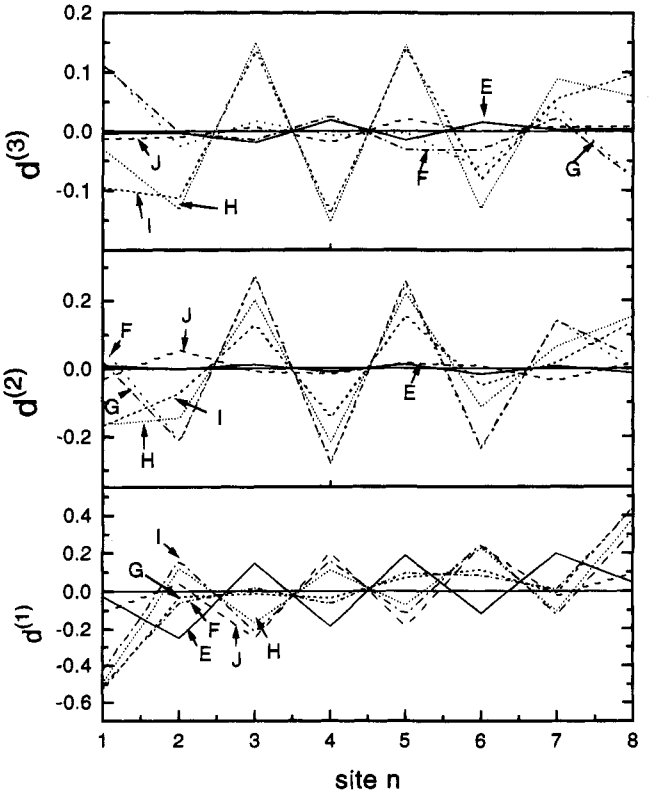

Figure 14. Induced charges for points E, F, G, H, I, and J: (a) first-order $d^{(1)}$; (b) second-order $d^{(2)}$; (c) third-order $d^{(3)}$.

An important feature of the coupled-oscillator picture is that it allows us to discuss separately the roles of the three

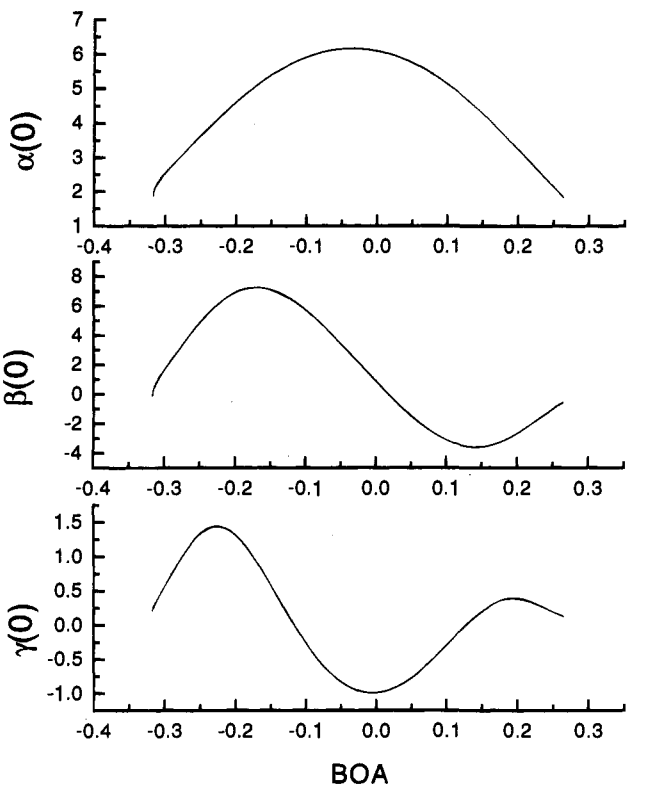

Figure 15. Off-resonant polarizabilities $\alpha(0)$, $\beta(0)$, and $\gamma(0)$ vs the bond order alternation (BOA).

Table 1. Sources of Nonlinearity for $\beta(0)$ and $\gamma(0)$ (10^{-28} and 10^{-33} esu, respectively)

point	X^a	C^a	D^a	X^b	C^b	D^b
E	0.169	−0.166	−0.418	−0.016	−0.011	0.137
G	1.213	−2.427	3.474	−0.451	0.205	−0.712
H	1.569	−4.343	10.033	1.554	−3.180	2.568
I	0.208	−2.288	8.291	1.496	−2.730	2.677
J	−0.113	0.060	−0.069	0.177	0.034	−0.002

[a] For $\beta(0)$. [b] For $\gamma(0)$.

anharmonic contributions: the nonlinear coupling to the external field, Coulomb coupling, and exchange coupling. To that end, we have carried out the following calculations: (I) the complete calculation with all anharmonic couplings included, (II) calculation that includes only the field and the Coulomb anharmonicities while the exchange coupling (X) is switched off, and (III) calculation that only includes the field nonlinearity, and both Coulomb (C) and exchange (X) terms are switched off. In all three cases, the values of $\alpha(0)$ are the same since it is not affected by the anharmonicities. However, $\beta(0)$ and $\gamma(0)$ change significantly. For instance, comparing cases I and II for point G, the value of $\beta(0)$ decreases from 2.3×10^{-28} to 1.0×10^{-28} esu, and $\gamma(0)$ changes from -0.96×10^{-33} to -0.50×10^{-33} esu, about a factor of 2. This indicates that the exchange coupling contribution is very significant.

In Table 1 we list contributions to $\beta(0)$ and $\gamma(0)$ from the three sources of anharmonic coupling. The exchange contribution, denoted X is the difference between (I) and (II). The Coulomb contribution, denoted C, is the difference between (II) and (III). The field contribution is denoted D and is given by (III). The total polarizability is the sum $X + C + D$. We list the values of X, C, and D for points E, G, H, I, and J. We find that X, C, and D are comparable and none can be neglected.

V. Dominant Oscillator Analysis

We have investigated the character of the harmonic oscillators. In Table 2 we list the frequencies Ω_ν, dipole moments

Table 2. Properties of the Electronic Harmonic Oscillators[a]

	1	2	3	4	5	6	7	8
Ω_ν	0	0	0	0	0	0	0	0
d_ν	1.840	0.889	0.155	0.369	1.610	0.994	0.364	1.247
f_ν	0	0	0	0	0	0	0	0
	9	10	11	12	13	14	15	16
Ω_ν	1.247	3.086	5.212	1.840	3.965	2.126	2.293	4.467
d_ν	0.376	1.825	0.271	0.287	1.012	0.688	1.941	0.126
f_ν	0	0	0	0	0	0	0	0
	17	18	19	20	21	22	23	24
Ω_ν	7.153	2.174	4.860	2.686	2.650	4.533	4.648	5.920
d_ν	0.565	1.699	0.629	4.855	4.670	0.280	0.472	0.432
f_ν	0	0	0	0	7.419	0.046	0.130	0.141
	25	26	27	28	29	30	31	32
Ω_ν	6.250	6.721	6.787	7.989	8.560	8.712	9.100	10.130
d_ν	0.286	0.077	0.205	0.227	0.292	0.084	0.037	0.041
f_ν	0.065	0.005	0.036	0.052	0.091	0.008	0.002	0.002
	33	34	35	36				
Ω_ν	10.840	11.722	13.099	15.439				
d_ν	0.048	0.007	0.008	0.004				
f_ν	0.003	0.000	0.000	0.000				

[a] Ω_ν is in units of eV and d_ν is in units of e·Å.

d_ν, and oscillator strengths f_ν of the electronic normal modes at point G. Note that the oscillator strengths f_ν for the first 20 oscillators vanish, which is why these modes do not participate in linear optical process. The dipole moments d_ν are finite for all oscillators. There are eight degenerate zero frequency modes and we have some freedom to construct them.

We shall now analyze our results using the oscillator picture.[6] In Figure 16, we display the oscillator strengths f_ν vs frequencies Ω_ν at points E, F, G, H, I, and J. In each panel, we also give the resulting effective mass m_0 (in units of the electron mass),[31] which is about twice the electron mass in all cases. Note that most oscillator strength accumulates in a single mode, which is consistent with the behavior of unsubstituted polyenes.[31] This mode is denoted the absorption mode (AM), and its frequency is the absorption peak frequency Ω_0. Mode 21 in Table 2 is the AM.

We next analyze the contribution of the various HO modes to the polarizabilities. We denote the contributions of the νth HO mode to $\alpha(0)$, $\beta(0)$, and $\gamma(0)$ as α_ν, β_ν, and γ_ν, respectively. Thus, we have $\alpha = \sum_\nu \alpha_\nu$, $\beta = \sum_\nu \beta_\nu$, and $\gamma_\nu = \sum_\nu \gamma_\nu$. The contribution of the νth mode to the nth order polarizability is equal to $d_\nu Q_\nu^{(n)}$, so that

$$\alpha_\nu = d_\nu Q_\nu^{(1)} \tag{51}$$

$$\beta_\nu = d_\nu Q_\nu^{(2)} \tag{52}$$

$$\gamma_\nu = d_\nu Q_\nu^{(3)} \tag{53}$$

In Figure 17 we plot α_ν vs Ω_ν. There is primarily only one harmonic oscillator (HO) mode (*i.e.*, the AM) contributing to $\alpha(0)$. At F and G, the AM's contribution to $\alpha(0)$ is the largest. This correlates well with the fact that $\alpha(0)$ attains its maximum around F and G.

In Figure 18 we plot β_ν vs Ω_ν. Here modes other than the AM contribute as well, especially a zero frequency mode (ZFM). At points E, F, G, and J, other modes have comparable contributions to those of AM and ZFM. However, these contributions are small compared to AM's and ZFM's contributions of points H and I. Thus, effectively only the AM and ZFM make a significant contribution to $\beta(0)$ at all points. This greatly simplifies the physical picture of $\beta(0)$. At H and I, AM and ZFM have large contributions.

Table 3. Index of Hartree–Fock Molecular Orbitals (HFMO) ($m = N/2$)

HFMO no.	configuration[a]	HFMO no.	configuration[a]
1	(p_1, h_1)	m^2+1	(h_1, p_1)
2	(p_1, h_2)	m^2+2	(h_2, p_1)
.	.	.	.
.	.	.	.
.	.	.	.
m^2	(p_m, h_m)	$2m^2$	(h_m, p_m)
$2m^2+1$	(h_1, h_2)	$3m^2-m+1$	(p_1, p_2)
$2m^2+2$	(h_1, h_3)	$3m^2-m+2$	(p_1, p_3)
.	.	.	.
.	.	.	.
.	.	.	.
$3m^2-m$	(h_m, h_{m-1})	$2m(2m-1)$	(p_m, p_{m-1})
$4m^2-2m+1$	(h_1, h_1)	$4m^2-m+1$	(p_1, p_1)
$4m^2-2m+2$	(h_2, h_2)	$4m^2-m+2$	(p_2, p_2)
.	.	.	.
.	.	.	.
.	.	.	.
$4m^2-m$	(h_m, h_m)	N^2	(p_m, p_m)

[a] $(q, r) = a_q^+ a_r$ where $q, r = p_i, h_j$ and $i, j = 1, 2, 3, 4$.

In Figure 19 we plot γ_ν vs Ω_ν. Many modes make small contributions to $\gamma(0)$ at E and J. At F and G there are four significant oscillators: AM, ZFM, a third mode (TM), and a fourth mode (FM). Mode 15 and mode 14 in Table 2 are TM and FM, respectively. At H and I, there is a large contribution from the ZFM. This leads to a maximum value of $\gamma(0)$. Another interesting observation is that the ZFM's contribution is positive at all points. The negative values at F and G come from AM, TM, and FM, and these lead to a minimum at F where the BOA vanishes.

We next introduce the Hartree–Fock molecular orbital (HFMO) representation. Details can be found in Appendix B and Table 3. The basis vector in HFMO is

$$|\hat{e}_{kk'}\rangle\rangle = a_k^+ a_{k'} \tag{54}$$

where a_k^+ ($a_{k'}$) is an electron creation (annihilation) operator ofthe Hartree–Fock molecular orbital k (k') in the absence of external field $\mathcal{E}$. We denote it (k, k') (see Table 3). So far we constructed our oscillators using two representations: the normal mode [eq 18] and real space [eq 32]. It is also possible to define oscillators corresponding to the Hartree–Fock molecular orbital basis set, denoted as the Hartree–Fock oscillator (HFO)

$$|\psi_\nu\rangle\rangle = \frac{1}{\sqrt{2}} \sum_{k<k'} S_{\nu,kk'} (a_k^+ a_{k'} + a_{k'}^+ a_k) \tag{55}$$

where $S_{\nu,kk'}$ is the expansion coefficient. We denote $(a_k^+ a_{k'} + a_{k'}^+ a_k)/\sqrt{2}$ as [k, k'] (see Table 4). To establish the connection with the traditional SOS method, we project the dominant modes onto the HFO representation. We chose point G where $\alpha(0)$ attains its maximum, $\beta(0) \approx 0$, BOA ≈ 0, and Ω_0 is close to its minimum. We projected the eigenfunctions of AM, ZFM, and TM onto the HFO representation (contributions from FM are usually smaller than those of TM, and thus we do not investigate them in detail). In Figure 20 we show the coefficient $S_{\nu,kk'}$ vs HFO's index for AM, ZFM, and TM. There are eight

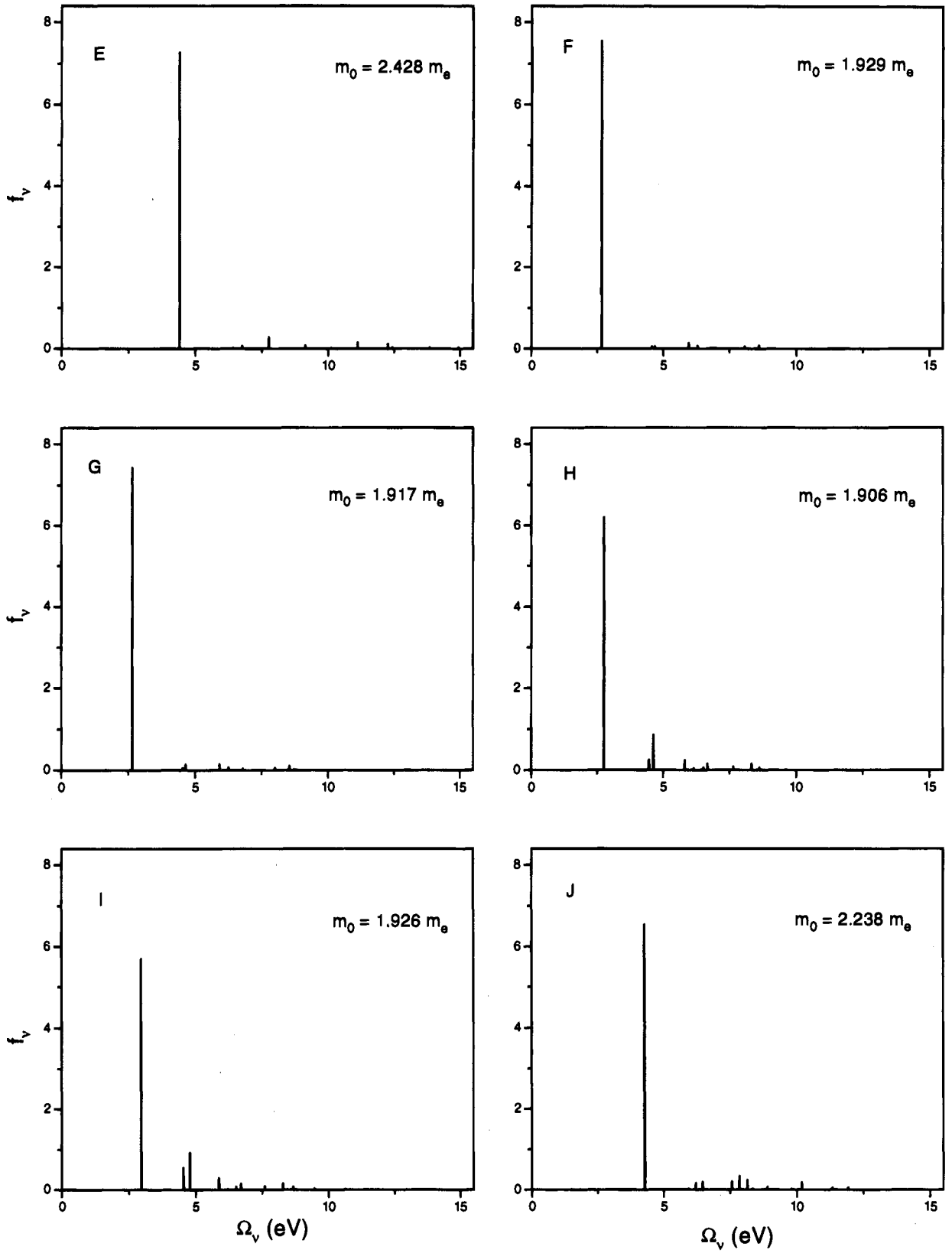

Figure 16. Oscillator strength vs frequencies for points E, F, G, H, I, and J. m_0 is the effective mass, and m_e is the electron mass.

zero-frequency oscillators. Because of this degeneracy, we have some freedom to lump all contributions to $\beta(0)$ or $\gamma(0)$ into a single radiative oscillator.[43] This oscillator has more than one component in the HFO representation and therefore acquires a collective nature. This important observation illustrates the ability of the HO picture to describe collective excitations. In principle, the ZFM eigenvector could be different in the second and third order. However, we found it to be very similar, and it is primarily made of $[h_4h_4]$ and $[p_1p_1]$ (Figure 20) excitation from LUMO–LUMO and HOMO–HOMO, respectively (p_1 represents LUMO and h_4 for HOMO, Figure 21). We have plotted the ZFM constructed from the second-order solution. It remains to be seen how general this conclusion is. If so, this

(43) Each zero frequency mode in Table 2 is chosen so that the majority of its components is a (p,p) or (h,h) mixed with small contributions from other components (h,p) and (p,h) (see Table 3 and Appendix B).

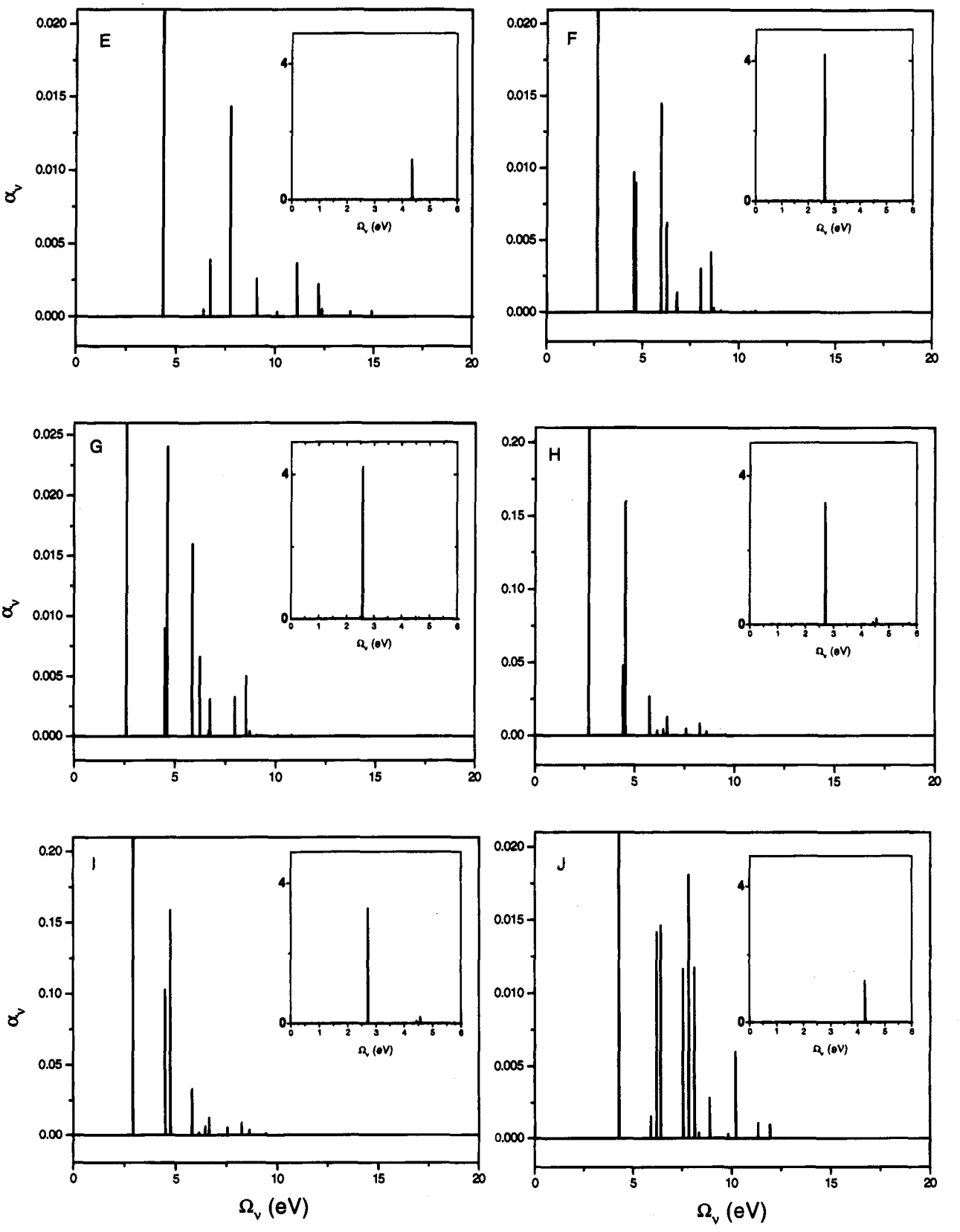

Figure 17. α_ν ((e·Å²)/*V*) vs Ω_ν for points E, F, G, H, I, and J. Since α_ν is dominated by a single AM mode (see insets), we have set the mode off scale to show the contributions of the other modes.

could provide a simple way to construct the ZFM. As shown in Figure 20, AM is made of $[p_1h_4]$, ZFM $[h_4h_4]$ and $[p_1p_1]$, and TM $[p_1h_4]$ and $[p_1p_2]$. FM is found to be mainly a combination of $[p_1h_4]$ and $[h_4h_3]$. In Table 5 we list the dominant HFOs of AM, ZFM, and TM at points E, F, G, H, I, and J. The coefficients are the amplitudes of HFO modes, and [p, h′], [p, p′], and [h, h′] stands for the dominant HFO modes.

The inverse participation ratio κ_ν of a harmonic oscillation ν is defined as

$$\kappa_\nu^{-1} \equiv \sum_{k,k'} |S_{\nu,kk'}|^4 \tag{56}$$

where ν is the index of the oscillator. κ_ν is roughly equal to

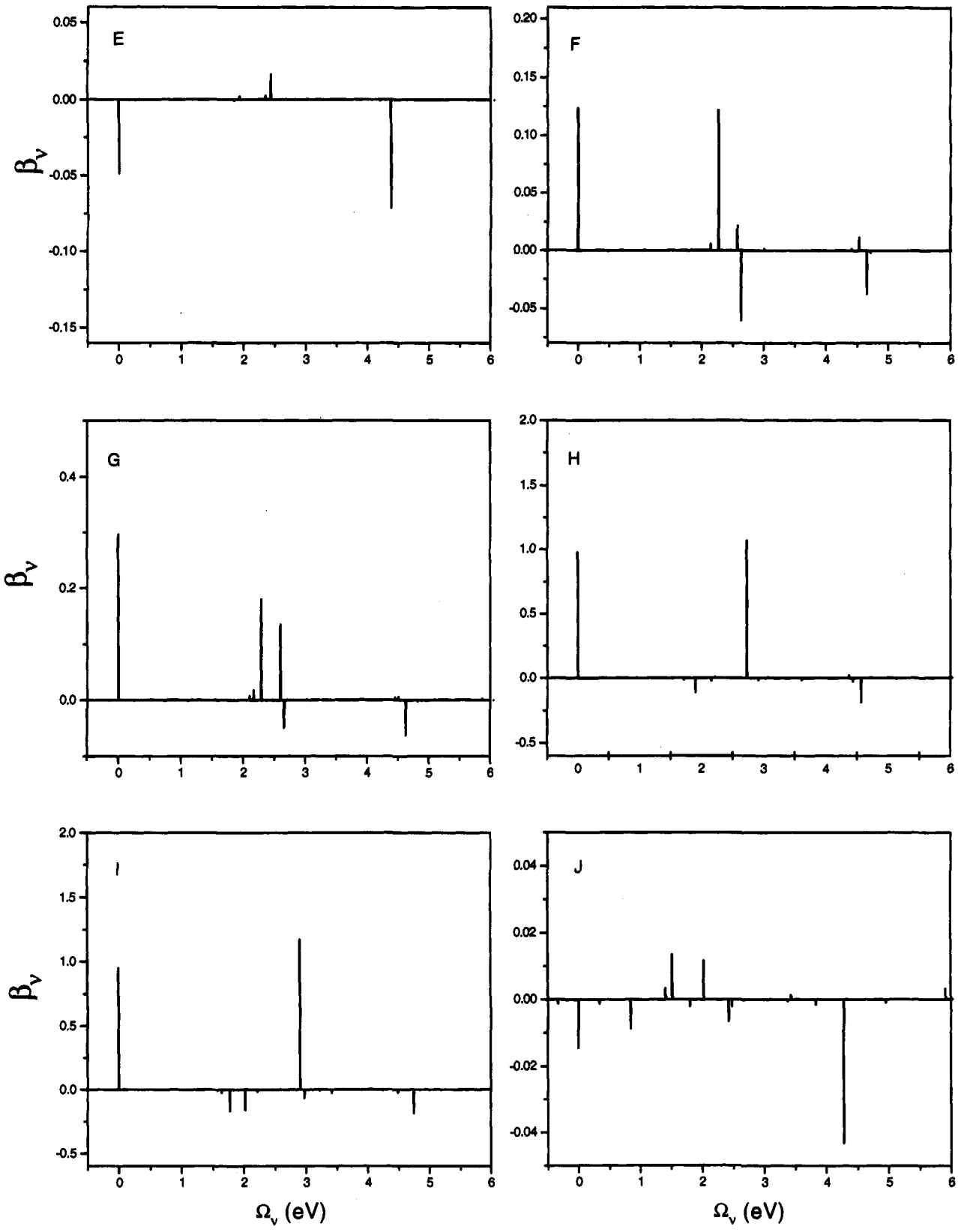

Figure 18. β_ν ((e·Å^3/V^2) vs Ω_ν for points E, F, G, H, I, and J. Besides AM, ZFM has a significant contribution.

the number of HFOs contributing to the νth oscillator, and we use it to characterize the distribution of harmonic oscillators in HFO. In Figure 22 we plot κ_ν at points G, H, and I. κ_ν of the ZFM is different in second and third order. However, we found that the difference is small in all cases: E, F, G, H, I, and J. In Figure 22 we plot ZFM's κ_ν of the second order. AM is made primarily of one HFO. TM and ZFM are made of two HFOs, reflecting their collective nature.

In Table 6 we list the dipole moment d_ν and the inverse participation ratio κ_ν of the dominant modes AM, ZFM, and TM, as well as their contributions to $\alpha(0)$, $\beta(0)$, and $\gamma(0)$. We also compare Ω_0 with the HOMO–LUMO energy difference. Note that Ω_0 is much smaller although the AM's eigenfunction is dominated by the transition between HOMO and LUMO. This red shift reflects the excitonic nature of the optical transition.[31] As shown in Appendix B, the diagonal element of the Liouville

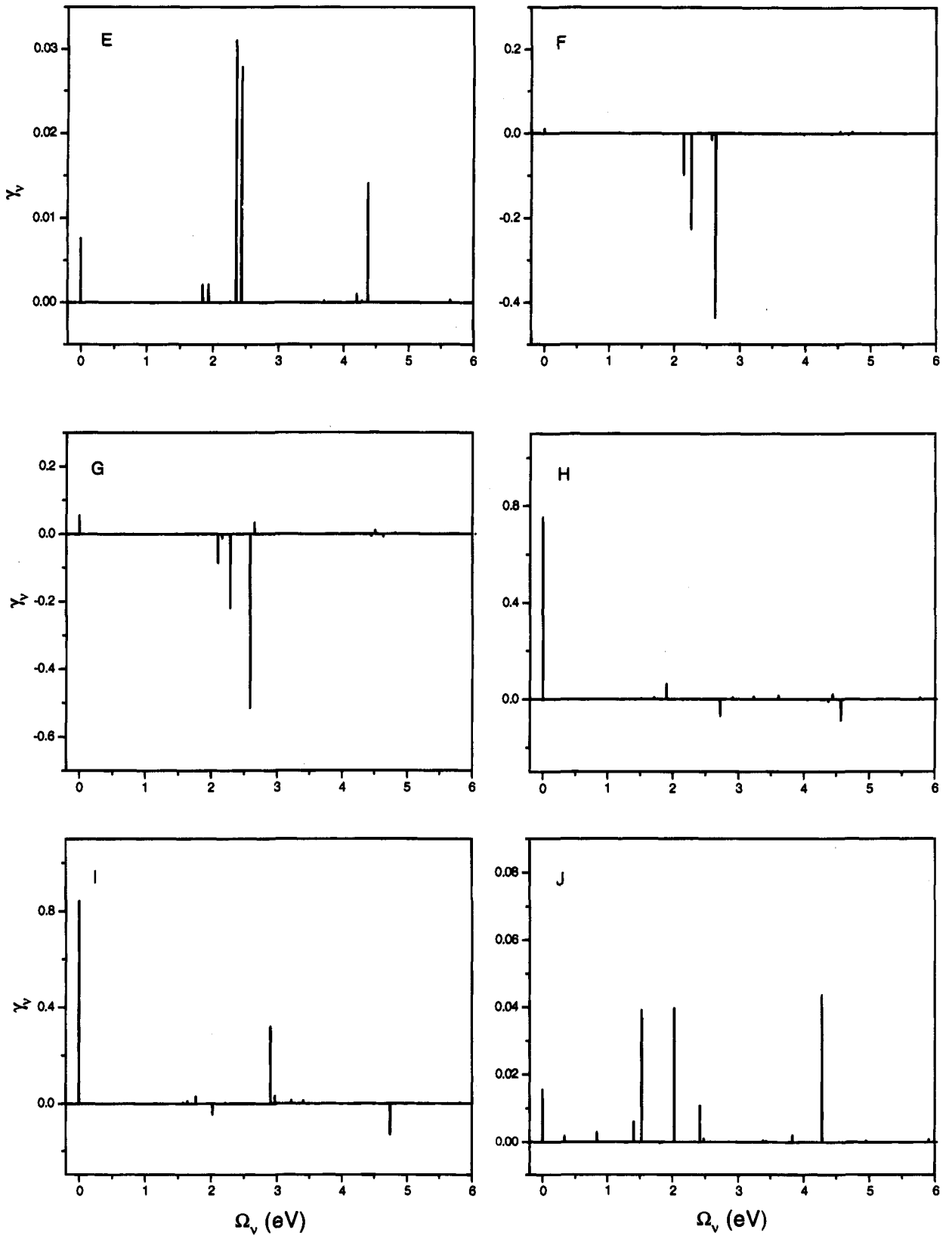

Figure 19. γ_ν ((e·Å^4/V^3) vs Ω_ν for points E, F, G, H, I, and J. Besides AM and ZFM, a third mode (TM) and a fourth mode (FM) have significant contributions.

operator in the Hartree–Fock molecular orbital (HFMO) representation is[6]

$$\tilde{\mathscr{L}}_{\mathrm{ph,ph}} = \xi_{\mathrm{p}} - \xi_{\mathrm{h}} + \tilde{v}_{\mathrm{ph,ph}} \tag{57}$$

and $\tilde{v}_{\mathrm{ph,ph}}$ is the Coulomb attractive interaction of an exciton.

VI. Summary and Discussion

In this paper we applied the coupled-oscillator picture to study conjugated polyenes substituted by a donor and an acceptor. We explored the relationships between the magnitudes of polarizabilities [$\alpha(0)$, $\beta(0)$, and $\gamma(0)$] and various other properties: BOA, charge transfer and absorption peak frequency Ω_0.

Table 4. Index of Hartree–Fock Oscillator (HFO)

HFO no.	configuration[a]	HFO no.	configuration[a]
1	$[p_1h_1]$	17	$[h_1h_2]$
2	$[p_1h_2]$	18	$[h_1h_2]$
.	.	.	.
.	.	.	.
.	.	.	.
16	$[p_4h_4]$	22	$[h_3h_4]$
23	$[p_1p_2]$	29	$[h_1h_1]$
24	$[p_1p_3]$	30	$[h_2h_2]$
.	.	.	.
.	.	.	.
.	.	.	.
28	$[p_3p_4]$	32	$[h_4h_4]$
33	$[p_1p31]$		
34	$[p_2p_2]$		
.	.		
.	.		
.	.		
36	$[p_4p_4]$		

[a] $[q, r] = (1/\sqrt{2})(a_q^+ a_r + a_r^+ a_q)$ where q, r = p_i, h_j and $i, j = 1, 2, 3, 4$.

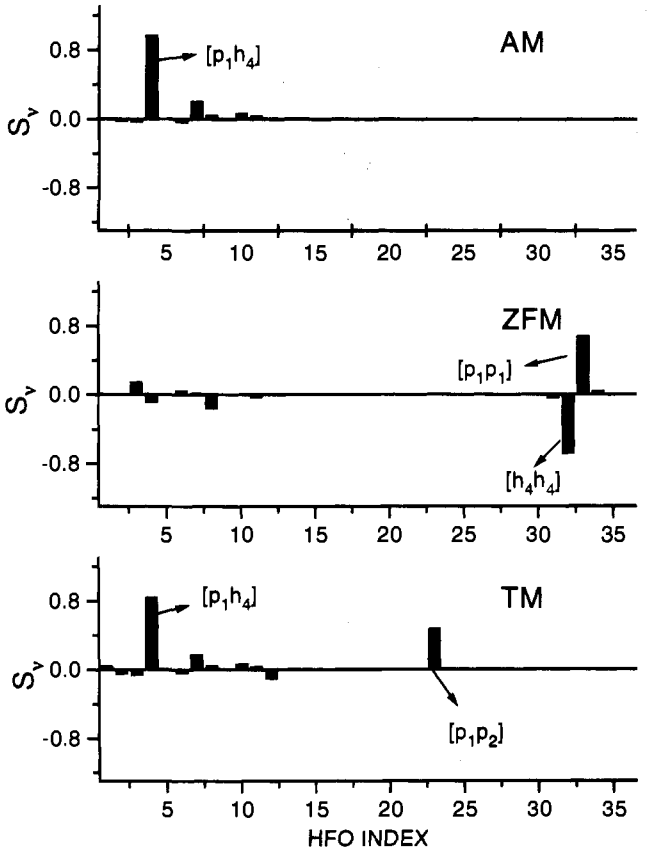

Figure 20. Projection of AM, ZFM, and TM onto HFO at point G. HFO stands for Hartree–Fock oscillators which are listed in Table 4. AM is made primarily of $[p_1h_4]$. ZFM is made mainly of $[h_4h_4]$ and $[p_1p_1]$. TM is made of $[p_1h_4]$ and $[p_1p_2]$.

Clear correlations among these parameters have been established. When BOA ≈ 0, Ω_0 is near its minimum and the value of $\alpha(0)$ is near its maximum. At BOA = 0, the π bonds are delocalized, and this helps electrons polarize along the entire chain, as seen in Figure 14. This maximizes the polarizability $\alpha(0)$. At this point, about half an electron transfers from donor to acceptor.

Strong variations of $\beta(0)$ and $\gamma(0)$ were also found. $\beta(0)$ goes through zero at BOA ≈ 0, and has one positive peak and one negative peak in the vicinity of that point. At large negative values of ϵ_D, there is a small peak along the ϵ_A axis (at $\epsilon_A \approx$ −6 eV). In this case the donor is decoupled from the rest of the system, and the system is effectively a hexatriene substituted with an acceptor at one end. The results of $\beta(0)$ are consistent with those of ref 9. $\gamma(0)$ has also one large positive peak, one small positive peak, and one large negative peak. However, further increase of donor–acceptor strength results in the decrease of $\alpha(0)$, $\beta(0)$, and $\gamma(0)$. $\alpha(0)$ is maximized in the vicinity of zero BOA, where the π bonds are delocalized. $\beta(0)$ and $\gamma(0)$ are maximized at finite values of BOA. All these provide some guidelines for optimizing the magnitudes of $\beta(0)$ and $\gamma(0)$. Earlier experiments indicated that an increase of the push–pull strength over a limited range resulted in the increase of $\beta(0)$.[44] Marder *et al.* measured the off resonant $\mu\beta$ and γ of six compounds and used solvents of different polarities to modify their donor and acceptor strengths.[8] Upon examining the variation of these quantities with the donor and acceptor strength, they found one positive peak and one negative peak for $\mu\beta$ and two positive peaks and one negative peak for γ. In the vicinity of the cyanine limit, $\mu\beta$ vanishes and γ attains a minimal value. Our results are consistent with these experimental observations.

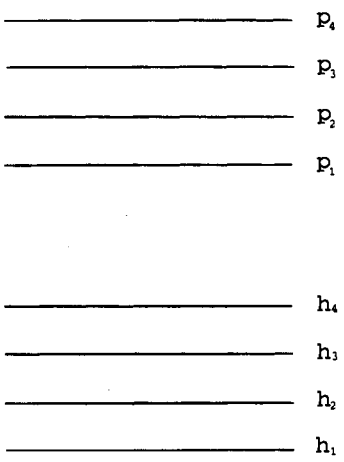

Figure 21. Hartree Fock levels of an $N = 8$ site system in particle–hole representation. p stands for particle and h for hole.

Table 5. Eigenfunctions of AM, ZFM, and TM

mode	point	1	2	3
AM	E	$0.6972[p_1h_4]$	$0.1099[p_2h_3]$	$0.0315[p_3h_2]$
	G	$0.6867[p_1h_4]$	$0.1483[p_2h_3]$	$0.0463[p_3h_2]$
	H	$0.6796[p_1h_4]$	$0.1128[p_2h_3]$	$0.1028[p_1h_3]$
	I	$0.6734[p_1h_4]$	$0.1349[p_1h_3]$	$0.1119[p_2h_4]$
	J	$0.6957[p_1h_4]$	$0.0905[p_2h_3]$	$0.0686[p_3h_3]$
ZFM[a]	E	$0.6820[h_4h_4]$	$0.6820[p_1p_1]$	$0.1225[p_2h_4]$
	G	$0.6869[h_4h_4]$	$0.6785[p_1p_1]$	$0.1175[p_2h_4]$
	H	$0.6940[h_4h_4]$	$0.661[p_1p_1]$	$0.1289[p_2h_4]$
	I	$0.7046[h_4h_4]$	$0.6522[p_1p_1]$	$0.1204[p_2p_2]$
	J	$0.6940[p_1p_1]$	$0.692[h_4h_4]$	$0.0908[p_1h_3]$
TM	E	$0.6390[p_1p_2]$	$0.2815[p_1h_4]$	$0.1003[p_3h_4]$
	G	$0.5967[p_1h_4]$	$0.3375[p_1p_2]$	$0.1235[p_2h_3]$
	H	$0.4814[p_1p_2]$	$0.4763[p_1h_4]$	$0.1459[p_1h_3]$
	I	$0.5745[p_1p_2]$	$0.3519[p_1h_4]$	$0.1565[p_1h_3]$
	J	$0.6844[p_1p_2]$	$0.1485[p_1h_4]$	$0.0773[p_3h_4]$

[a] Second-order solution.

The electronic normal mode representation can differentiate between various sources of nonlinearities. We studied separately the roles of Coulomb (C), exchange (X) and field (D) nonlinear couplings and found that none is dominant. The ability to relate these couplings directly to the optical response (and not through the eigenstates) is a major advantage of the present picture.

We also connected the coupled harmonic oscillator picture to the traditional SOS approach by projecting the harmonic

(44) Oudar, J. L. *J. Chem. Phys.* **1977**, *67*, 446.

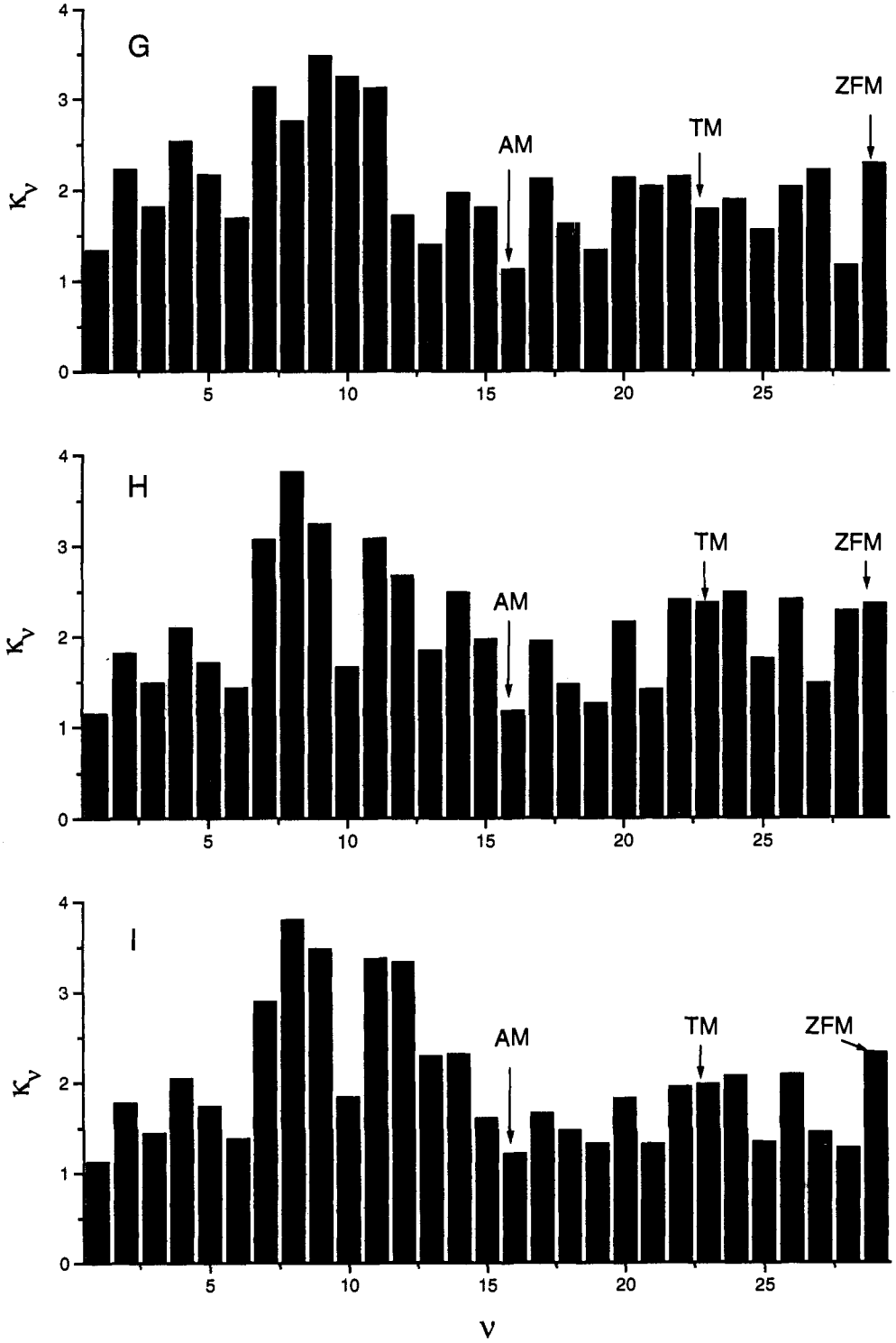

Figure 22. Inverse participation ratio κ_ν vs ν for points G, H, and I. ν is the index of HO. ZFM corresponds to the second-order calculation. AM consists mainly of one HFO. TM and ZFM are made of two HFOs.

oscillators onto the HFO representation and calculating the inverse participation ratio κ_ν. This reveals the collective nature of the electronic oscillators. We investigated the character of the dominant oscillators and identified what molecular orbital transitions they represent. We found that four electronic oscillators, AM, ZFM, TM, and FM, contribute significantly to the off-resonant polarizabilities $\alpha(0)$, $\beta(0)$, and $\gamma(0)$. They represent transitions among the following molecular orbitals: p_1, p_2, h_4, and h_3, *i.e.*, the first and second LUMO, and the first and second HOMO. It remains to be seen how this picture changes for the resonant response.

Currently the coupled harmonic oscillator picture is based on the TDHF. Single ph/hp excitations have been accounted for explicitly. Further analysis reveals that double excitations have been partially taken into account as well.[45] TDHF starts from the static Hartree–Fock ground state which does not include electron–electron correlations. A natural extension will be to start from a ground state which incorporates essential electron–electron correlations, and then to follow the motions of electron–hole pairs. The coupled-cluster equation of motion (CC-EOM)[46-48] accomplishes this goal. Both the coupled

(45) Bonacic-Koutecky, V.; Fantucci, P.; Koutecky, J. *Chem. Rev.* **1991**, *91*, 1035.
(46) Rowe, D. J. *Rev. Mod. Phys.* **1968**, *40*, 153.
(47) (a) Shibuya, T.-I.; McKoy, V. *Phys. Rev. A* **1970**, *2*, 2208. (b) Shibuya, T.-I.; Rose, J.; McKoy, V. *J. Chem. Phys.* **1973**, *58*, 500.

Table 6. Characters of AM, ZFM, and TM

mode	point	μ_ν[c] (eV)	d_ν (e·Å)	κ_ν	α_ν[a]	β_ν[a]	γ_ν[a]
AM	E	4.4128 (7.5742)	3.2009	2.11	1.1718	−0.0690	0.1435
	F	2.6734 (5.0931)	4.6744	2.24	4.1776	−0.0606	−0.4361
	G	2.6499 (5.0456)	4.6696	2.24	4.2072	0.1348	−0.5142
	H	2.7533 (5.0680)	3.9174	2.34	3.2700	1.0657	−0.0673
	I	2.9638 (5.2953)	3.8820	2.42	2.5730	1.1706	0.3206
	J	4.2827 (7.3720)	3.2096	2.13	1.2172	−0.0431	0.0436
ZFM[b]	E	0	0.8526	2.30	0	−0.0487	0.0076
	F	0	0.3915	2.25	0	0.1236	0.0102
	G	0	0.9178	2.29	0	0.2957	0.0542
	H	0	3.7939	2.35	0	0.9755	0.7511
	I	0	4.9697	2.33	0	0.9497	0.8416
	J	0	0.2400	2.17	0	−0.0145	0.0156
TM	E	2.4194	2.9121	2.89	0	0.0020	0.0310
	F	2.3055	1.8734	3.58	0	0.1216	−0.2260
	G	2.2932	1.9406	3.57	0	0.1793	−0.2188
	H	2.1765	0.1517	4.74	0	−0.0180	−0.0011
	I	2.0359	1.6901	3.96	0	−0.1585	−0.0433
	J	1.5769	3.4343	2.27	0	0.0135	0.0390

[a] α_ν is in units of 10^{-22} esu, β_ν is in units of 10^{-28} esu, and γ_ν is in units of 10^{-33} esu. [b] The wave function of ZFM is the second-order solution. [c] Data in parentheses are the energy differences between LUMO and HOMO, and those on the top are the frequency Ω_ν for oscillator ν.

harmonic oscillator technique and the CC-EOM follow the motions of electron–hole pairs. Thus, it is straightforward to combine the two approaches. Another approach that goes beyond TDHF approximation was proposed by Linderberg and Ohrn,[35] based on the work of Hubbard.[49] It follows the motion of the electron propagator as well as some correlation functions, and thus includes electronic correlations. The Slave–Boson technique introduces some bosonic fields and connects them to specific electron–electron correlations.[50] For the Hubbard model, its mean-field solution is found to be exactly that of the Gutzwiller approximation.[51] Starting from the mean-field ground state and following the dynamics of the electron–hole pair as well as those of bosons, one can derive a set of coupled equations of motion for electrons and bosons.[52] Further studies are necessary to determine the relevance of these approaches to optical processes of the conjugated systems. The one-dimensional Hubbard model has been investigated extensively. It is the strong correlation limit of the PPP Hamiltonian. Its ground state has been solved by Lieb and Wu,[53] and lately its full excitation spectrum has been obtained.[54] These exact solutions of the 1D Hubbard model can help clarify the correlated nature of the PPP Hamiltonian, and thus lead to a better understanding of the optical properties of conjugated polymers.

In order to interpret the resonant spectroscopy of conjugated polyenes, we need to take nuclear motions into account. Apart from vibronic transitions, these induce large lattice distortions (soliton and polaron)[55,56] as well as an inhomogeneous distribution of configurations. We believe that the electronic oscillator method when combined with techniques such as the Car–Parrinello procedure[57] is particularly suitable to address these issues.

Acknowledgment. We wish to thank Dr. V. Chernyak, Dr. A. Takahashi, and Dr. S. Marder for stimulating discussions and useful comments. The support of the Air Force office of scientific research, the National Science Foundation, and the Center for Photoinduced Charge Transfer is gratefully acknowledged.

Appendix A: Harmonic Oscillator Representation

In this appendix we derive eqs 23, 29, and 30. From eq 17, we obtain the following symmetry relationship among the elements of matrix $\mathscr{L}$:

$$\mathscr{L}_{ij,mn} = -\mathscr{L}_{ji,nm} \tag{A1}$$

Assuming that an eigenvector of eq 18 $|\psi_\nu\rangle\rangle = \sum_{mn} \mathscr{U}^1_{mn,\nu}|\hat{e}_{nm}\rangle\rangle$ and its eigenvalue is $\hbar\Omega_\nu$, we have the following equation:

$$\hbar\Omega_\nu \mathscr{U}^1_{ij,\nu} - \sum_{mn} \mathscr{L}_{ij,mn} \mathscr{U}^1_{mn,\nu} = 0 \tag{A2}$$

Denoting $\mathscr{U}^1_{ij,\nu} \equiv \mathscr{U}^1_{ji,\bar{\nu}}$ and $\Omega_\nu \equiv -\Omega_{\bar{\nu}}$, and using eq A1, we have

$$\hbar\Omega_\nu \mathscr{U}^1_{ij,\nu} + \sum_{mn} \mathscr{L}_{ji,nm} \mathscr{U}^1_{mn,\nu} = 0 \tag{A3}$$

Thus, we find another eigenvector $|\psi_{\bar{\nu}}\rangle\rangle = \sum_{mn} \mathscr{U}^1_{mn,\bar{\nu}}|\hat{e}_{nm}\rangle\rangle$, where

$$\mathscr{U}^1_{mn,\nu} = \mathscr{U}^1_{nm,\bar{\nu}} \tag{A4}$$

and its eigenvalue $\Omega_{\bar{\nu}} = -\Omega_\nu$. Further we find that

$$\mathscr{U}_{\nu,mn} = \mathscr{U}_{\bar{\nu},nm} \tag{A5}$$

Multipling eq 17 by $\mathscr{U}$ from the left and using eq 22, we obtain

$$i\hbar\delta\dot{\varrho}_\nu - \hbar\Omega_\nu\delta\varrho_\nu = [\bar{f}, \varrho^{(0)}]_\nu + [\bar{f}, \delta\varrho]_\nu + [\delta h, \delta\varrho]_\nu \tag{A6}$$

Substituting $\delta\varrho_{mn} = \sum_\nu \mathscr{U}^1_{mn,\nu}\delta\varrho_\nu$, we find

$$[\bar{f}, \varrho^{(0)}]_\nu = \mathscr{E}E_\nu \tag{A7}$$

$$[\bar{f}, \delta\varrho]_\nu = \mathscr{E}\sum_{\nu'} F_{\nu,\nu'}\delta\varrho_{\nu'} \tag{A8}$$

$$[\delta h, \delta\varrho]_\nu = \sum_{\nu'\nu''} (J_{\nu,\nu'\nu''} + K_{\nu,\nu'\nu''})\delta\varrho_{\nu'}\,\delta\varrho_{\nu''} \tag{A9}$$

where

$$E_\nu = \sum_{mn} e[z(m) - z(n)]\,\mathscr{U}_{\nu,mn}\varrho^{(0)}_{mn} \tag{A10}$$

$$F_{\nu,\nu'} = \sum_{mn} e[z(m) - z(n)]\,\mathscr{U}_{\nu,mn}\mathscr{U}^1_{mn,\nu'} \tag{A11}$$

$$J_{\nu,\nu',\nu''} = \sum_{mn,k} 2(v_{mk} - v_{nk})\,\mathscr{U}_{\nu,mn}\mathscr{U}^1_{kk,\nu'}\mathscr{U}^1_{mn,\nu''} \tag{A12}$$

(48) Sekino, H.; Bartlett, R. J. *Int. J. Quantum Chem., Quantum Chem. Symp.* **1984**, *S18*, 255.
(49) (a) Hubbard, J. *Proc. R. Soc. London* **1963**, *A276*, 238. (b) Hubbard, J. *Proc. R. Soc. London* **1967**, *A296*, 100.
(50) (a) Barnes, S. E. *J. Phys. F* **1976**, *6*, 1375. (b) Barnes, S. E. *J. Phys. F* **1977**, *7*, 2937. (c) Coleman, P. *Phys. Rev. B* **1984**, *29*, 3035.
(51) Kotliar, G.; Ruckenstein, A. E. *Phys. Rev. Lett.* **1986**, *57*, 1362.
(52) Chen, G.; Mukamel, S. Work in progress.
(53) (a) Lieb, E.; Wu, F. Y. *Phys. Rev. Lett.* **1968**, *20*, 1445. (b) Yang, C. N. *Phys. Rev. Lett.* **1967**, *19*, 1315.
(54) (a) Essler, F. H. L.; Korepin, V. E.; Schoutens, K. *Phys. Rev. Lett.* **1991**, *67*, 3848. (b) Audit, P. *J. Phys. A* **1990**, *23*, L389.
(55) Heeger, A. J.; Kivelson, S.; Schrieffer, J. R.; Su, W. P. *Rev. Mod. Phys.* **1988**, *60*, 781.
(56) Hagler, T. W.; Heeger, A. J. *Chem. Phys. Lett.* **1992**, *189*, 333.
(57) Car, R.; Parrinello, M. *Phys. Rev. Lett.* **1985**, *55*, 2471.

$$K_{\nu,\nu',\nu''} = \sum_{mn,k} (-1)(\nu_{mk} - \nu_{nk})\, \mathcal{U}_{\nu,mn}\, \mathcal{U}^{-1}_{mk,\nu'}\, \mathcal{U}^{-1}_{kn,\nu''} \quad \text{(A13)}$$

We thus obtain the EOM (eq 23) in the HO representation.

The EOM for $\delta\varrho_{\bar\nu}$ can be written as

$$i\hbar\delta\dot\varrho_{\bar\nu} = \hbar\Omega_{\bar\nu}\delta\varrho_{\bar\nu} = [\bar f, \varrho^{(0)}]_{\bar\nu} + [\bar f, \delta\varrho]_{\bar\nu} + [\delta h, \delta\varrho]_{\bar\nu} \quad \text{(A14)}$$

Combining eqs A6 and A14, we obtain the EOM (eqs 29 and 30) for Q_ν and P_ν. The coefficients $\bar E$, C, X, and D in eqs 29 and 30 are

(1) for $\Omega_\nu \neq 0$

$$\bar E_\nu = -\sqrt{2}e\hbar^{-1}\sum_{mn}[z(m) - z(n)]\, \mathcal{U}_{\nu,mn}\varrho^{(0)}_{mn}$$

$$D^{a}_{\nu,\nu'} = \hbar^{-1}(F_{\nu,\nu'} + F_{\nu,\bar\nu'})$$

$$D^{b}_{\nu,\nu'} = \hbar^{-1}(F_{\nu,\nu'} - F_{\nu,\bar\nu'})$$

$$C^{a}_{\nu,\nu'\nu''} = \sqrt{2}\hbar^{-1}(J_{\nu,\nu'\nu''} + J_{\nu,\nu'\bar\nu''})$$

$$C^{b}_{\nu,\nu'\nu''} = \sqrt{2}\hbar^{-1}(J_{\nu,\nu'\nu''} - J_{\nu,\nu'\bar\nu''})$$

$$X^{a}_{\nu,\nu'\nu''} = (\sqrt{2}/2)\hbar^{-1}(K_{\nu,\nu'\nu''} + K_{\nu,\nu'\bar\nu''} + K_{\nu,\bar\nu'\nu''} + K_{\nu,\bar\nu'\nu''})$$

$$X^{b}_{\nu,\nu'\nu''} = (\sqrt{2}/2)\hbar^{-1}(K_{\nu,\nu'\nu''} + K_{\nu,\nu''\nu'} - K_{\nu,\nu'\bar\nu''} + K_{\nu,\nu''\bar\nu'} + K_{\nu,\bar\nu'\nu''} - K_{\nu,\bar\nu''\nu'} - K_{\nu,\bar\nu'\nu''} - K_{\nu,\bar\nu''\bar\nu'})$$

$$X^{c}_{\nu,\nu'\nu''} = (\sqrt{2}/2)\hbar^{-1}(K_{\nu,\nu'\nu''} - K_{\nu,\nu'\bar\nu''} - K_{\nu,\bar\nu'\nu''} + K_{\nu,\bar\nu'\bar\nu''}) \quad \text{(A15)}$$

(2) for $\Omega_\mu = 0$

$$D^{a}_{\mu,\nu'} = (1/2)\hbar^{-1}(F_{\mu,\nu'} + F_{\mu,\bar\nu'})$$

$$D^{b}_{\mu,\nu'} = (1/2)\hbar^{-1}(F_{\mu,\nu'} - F_{\mu,\bar\nu'})$$

$$C^{a}_{\mu,\nu'\nu''} = (\sqrt{2}/2)\hbar^{-1}(J_{\mu,\nu'\nu''} + J_{\mu,\nu'\bar\nu''})$$

$$C^{b}_{\mu,\nu'\nu''} = (\sqrt{2}/2)\hbar^{-1}(J_{\mu,\nu'\nu''} - J_{\mu,\nu'\bar\nu''})$$

$$X^{a}_{\mu,\nu'\nu''} = (\sqrt{2}/4)\hbar^{-1}(K_{\mu,\nu'\nu''} + K_{\mu,\nu'\bar\nu''} + K_{\mu,\bar\nu'\nu''} + K_{\mu,\bar\nu'\bar\nu''})$$

$$X^{b}_{\mu,\nu'\nu''} = (\sqrt{2}/4)\hbar^{-1}(K_{\mu,\nu'\nu''} + K_{\mu,\nu''\nu'} - K_{\mu,\nu'\bar\nu''} + K_{\mu,\nu''\bar\nu'} + K_{\mu,\bar\nu'\nu''} - K_{\mu,\bar\nu''\nu'} - K_{\mu,\bar\nu'\bar\nu''} - K_{\mu,\bar\nu''\bar\nu'})$$

$$X^{c}_{\mu,\nu'\nu''} = (\sqrt{2}/4)\hbar^{-1}(K_{\mu,\nu'\nu''} - K_{\mu,\nu'\bar\nu''} - K_{\mu,\bar\nu'\nu''} + K_{\mu,\bar\nu'\bar\nu''}) \quad \text{(A16)}$$

Using the symmetry relationships A4 and A5, we obtain

$$P_\nu(\omega) \propto \omega \quad \text{(A17)}$$

as $\omega \to 0$.

Appendix B: Hartree–Fock Molecular Orbital Representation

In HFMO representation, eq 17 becomes[6]

$$i\hbar\delta\dot{\boldsymbol{\varrho}} - \tilde{\mathcal{L}}\delta\boldsymbol{\varrho} = [\bar{\mathbf{f}}, \boldsymbol{\varrho}^{(0)}] + [\bar{\mathbf{f}}, \delta\boldsymbol{\varrho}] + [\delta\mathbf{h}, \delta\boldsymbol{\varrho}] \quad \text{(B1)}$$

where

$$\tilde{\mathcal{L}} = \mathcal{V}\mathcal{L}\mathcal{V}^{-1} \quad \text{(B2)}$$

$$\mathcal{V}_{kk',mn} = c_{mk}c_{nk'} \quad \text{(B3)}$$

c_{mk} ($c_{mk'}$) is the normalized HFMO coefficient of the HF orbital k (k′) at atom m (n), and

$$\tilde{\mathcal{L}}_{ph,p'h'} = (\epsilon_p - \epsilon_h)\delta_{p,p'}\delta_{h,h'} + \tilde v_{ph,p'h'} \quad \text{(B4)}$$

$$\tilde{\mathcal{L}}_{ph,h'p'} = \tilde v_{ph,h'p'} \quad \text{(B5)}$$

$$\tilde{\mathcal{L}}_{ph,h'h''} = \tilde v_{ph,h'h''} \quad \text{(B6)}$$

$$\tilde{\mathcal{L}}_{ph,p'p''} = \tilde v_{ph,p'p''} \quad \text{(B7)}$$

$$\tilde{\mathcal{L}}_{pp',p''p'''} = \tilde{\mathcal{L}}_{hh',h''h'''} = \tilde{\mathcal{L}}_{pp',hh'} = 0 \quad \text{(B8)}$$

$$\tilde{\mathcal{L}}_{ph,p'h'} = -\tilde{\mathcal{L}}_{hp,h'p'} \quad \text{(B9)}$$

$$\tilde{\mathcal{L}}_{ph,h'p'} = -\tilde{\mathcal{L}}_{h'p',ph} \quad \text{(B10)}$$

$$\tilde{\mathcal{L}}_{ph,h'h''} = -\tilde{\mathcal{L}}_{hp,h''h'} \quad \text{(B11)}$$

$$\tilde{\mathcal{L}}_{ph,p'p''} = -\tilde{\mathcal{L}}_{hp,p''p'} \quad \text{(B12)}$$

where

$$\tilde v_{kk',k''k'''} = \sum_{mn}(2\,\mathcal{V}_{kk',mm}\,\mathcal{V}_{k''k''',nm} - \mathcal{V}_{kk',mn}\,\mathcal{V}_{k''k''',mn})v_{nm} \quad \text{(B13)}$$

The labeling of the HFMO is shown in Figure 21. We arrange HFMO transitions in the following order: ph, hp, hh′/h′h, pp′/p′p, hh/hh and pp/pp. In Figure 21 we plot the energy levels of Hartree–Fock molecular orbitals. p stands for the unoccupied orbitals and h stands for the occupied orbitals. In Table 3, we list the index of the Hartree–Fock molecular orbital transitions. Using this index $\tilde{\mathcal{L}}$ has the following form:

$$\tilde{\mathcal{L}} = \begin{pmatrix} \tilde{\mathcal{L}}_1 & \mathbf{C} \\ 0 & \boldsymbol{\Omega}_2 \end{pmatrix} \quad \text{(B14)}$$

$$\tilde{\mathcal{L}}_1 = \begin{pmatrix} \mathbf{A} & \mathbf{B} \\ -\mathbf{B} & -\mathbf{A} \end{pmatrix} \quad \text{(B15)}$$

where $\mathbf{A}$ and $\mathbf{B}$ are $N^2/4 \times N^2/4$ matrices and N is the number of sites. $\boldsymbol{\Omega}_2$ is a $N^2/2 \times N^2/2$ diagonal matrix, and its diagonal elements are given by the differences of the HF eigenvalues. $\mathbf{C}$ is an $N^2/2 \times N^2/2$ matrix,

$$\mathbf{C} = \begin{pmatrix} \tilde{\mathcal{L}}_{ph,kk'} \\ \tilde{\mathcal{L}}_{hp,kk'} \end{pmatrix} \quad \text{(B16)}$$

where kk′ = hh′ or pp′.

With these definitions, it is easy to prove the following:[6,37] (1) $N^2/2$ HO modes consist only of ph and hp components of ϱ. (2) Frequencies of other $N^2/2$ HO modes are identical to the diagonal elements of $\boldsymbol{\Omega}_2$. These include N zero frequency modes (ZFM). (3) Except for the ZFM, every HO mode ν has its conjugate mode $\bar\nu$ so that $\Omega_\nu = -\Omega_{\bar\nu}$.

JA9430154